~~Street-in-Grid~~ Non-stationary modeling of ~~gas-phase pollutants~~ NO_2, NO and NO_x in Paris city using Street-in-Grid model: coupling local and regional scales with a two-way dynamic approach

Lya Lugon[1,2], Karine Sartelet[1], Youngseob Kim[1], Jérémy Vigneron[3], and Olivier Chrétien[2]

[1]CEREA, Joint Laboratory École des Ponts ParisTech/EDF R&D, Université Paris-Est, 77455 Champs-sur-Marne, France
[2]Paris City, Department of green spaces and environment, 103 Avenue de France, France
[3]Airparif, France

Correspondence: Lya Lugon (lya.lugon@enpc.fr), Karine Sartelet (karine.sartelet@enpc.fr)

Abstract. Regional-scale chemistry-transport models have coarse spatial resolution (coarser than 1 km x 1 km), and thus can only simulate background concentrations. They fail to simulate the high concentrations observed close to roads and in streets, ~~i.e.~~ where a large part of the urban population lives. Local-scale models may be used to simulate concentrations in streets. They often assume that background concentrations are constant and/or use simplified chemistry. Recently developed, the multi-scale model Street-in-Grid (SinG) estimates gaseous pollutant concentrations simultaneously at local and regional scales, coupling them dynamically. This coupling combines the regional-scale chemistry-transport model Polair3D and the street network model ~~MUNICH (~~Model of Urban Network of Intersecting Canyons and Highway ~~)~~(MUNICH) with a two-way feedback. MUNICH models explicitly street canyons and intersections, and it is coupled to the first vertical level of the chemical-transport model, enabling the transfer of pollutant mass between the street canyon roof and the atmosphere. The original versions of SinG and MUNICH adopt a stationary hypothesis to estimate pollutant concentrations in streets. Although the computation of NO_x concentration is numerically stable with the stationary approach, the partitioning between NO and NO_2 is highly dependent on the time step of coupling between transport and chemistry processes. In this study, a new non-stationary approach is presented with a fine coupling between transport and chemistry, leading to numerically stable partitioning between NO and NO_2. Simulations of NO, NO_2 and NO_x concentrations over Paris city with SinG, MUNICH and Polair3D are compared to observations at traffic and urban stations to estimate the added value of multi-scale modeling with a two-way dynamical coupling between the regional and local scales. As expected, the regional chemical-transport model underestimates NO and NO_2 concentrations in the streets. However, there is a good agreement between the measurements and the concentrations simulated with MUNICH and SinG. The two-way dynamic coupling between the local and regional scales tends to be important for streets with an intermediate aspect ratio and with high traffic emissions.

1 Introduction

Air pollution is a serious problem in many cities due to its considerable impacts on human health and the environment, as reported in WHO (2006), Brønnum-Hansen et al. (2018), Lee et al. (2018), Chen et al. (2019), Katoto et al. (2019), De Marco

et al. (2019). These impacts motivated the development of air-quality models, that estimate pollutant dispersion at determined spatial scales. These models are largely employed to calculate the population exposure and they can support public strategies for pollution control.

Regional-scale chemistry-transport models (CTMs), as three-dimension gridded Eulerian models ~~(e.g. Polair3D (Sartelet et al., 2007), WRF-Chem (Zhang et al., 2010), CHIMERE (Menut et al., 2014), CMAQ (Community Multi-scale Air Quality Modeling System) (Byun and Ching, 1999), AURORA (Mensink et al., 2001))~~ solve a chemistry-transport equation for chemical compounds or surrogates, taking into account pollutant emissions, transport (advection by winds, turbulent diffusion), chemical transformations, and dry/wet depositions. Several CTMs are available in the literature, e.g., Polair3D, WRF-Chem, CHIMERE, Community Multi-scale Air Quality Modeling System (CMAQ), Air Quality Model For Urban Regions Using An Optimal Resolution Approach (AURORA), described in Sartelet et al. (2007); Zhang et al. (2010); Menut et al. (2014); Byun and Ching (1999); Me
The simulated concentrations at each grid cell are averaged over the whole cell surface, often with resolution coarser than 1 km^2. CTMs are largely employed to simulate background concentrations, but they are not able to represent the gradients of concentrations observed between near-traffic areas and background. Indeed, in streets, for several pollutants, the concentrations are considerably higher than background ones, due to the proximity of traffic emissions and reduced natural ventilation. It is the case for NO_2, for example, which is emitted by traffic and also formed in the atmosphere. Therefore, many street-network models were formulated specifically in the last decades to estimate pollutant concentrations at the local scale more accurately, with a relatively low computational cost.

The first street-network models were the STREET model (Johnson et al., 1973) and the Hotchkiss and Harlow model (Hotchkiss and Harlow, 1973). The STREET model uses a very simplified parametrization, where the concentration in a street is assumed to be the sum of a street contribution (c_s) generated by traffic emissions and a background contribution (c_b). STREET was formulated using empirical parameters based on measurements performed in streets of San Jose and St. Louis. The Hotchkiss and Harlow model is an analytical street-canyon model. It implements an approximate solution of the steady-state advection-diffusion equation, using an eddy diffusivity formulation to describe pollutant dispersion. However, this model assumes a square-root dependency between pollutant dilution and the distance from the source, which may not be appropriate in street canyons, where source-receptor distances are short (Berkowicz et al., 1997).

~~Afterward,~~

Other street-network models ~~, such as CALINE4 (California Line source dispersion model) (Benson, 1984), (Sharma et al., 2013) and CAR (Calculation of Air pollution from Road traffic model) (Eerens et al., 1993),~~ assume that pollutant dispersion follows a Gaussian plume distribution and ~~traffic emissions are line sources~~consider traffic emissions as line sources, as the Calculation of Air pollution from Road traffic model (CAR) and the California Line source dispersion model (CALINE4), developed by Eerens et al. (1993) and Sharma et al. (2013) respectively. Other models expanded this formulation combining a Gaussian plume and a box model, e.g.~~CPBM (~~, the Canyon Plume Box Model ~~) (Yamartino and Wiegand, 1986), OSPM (~~(CPBM), the Operational Street Pollution Model ~~) (Berkowicz et al., 1997; Berkowicz, 2000), and ADMS-Urban (~~(OSPM), and the urban version of Atmospheric Dispersion Modeling System ~~) (McHugh et al., 1997)~~(ADMS-Urban). The Gaussian plume model is

used to estimate the direct contribution of traffic emissions, and the box model calculates the recirculation contribution, resultant from the wind vortex formed in the street canyon (Yamartino and Wiegand, 1986; Berkowicz et al., 1997; Berkowicz, 2000; McHugh e

With a different approach, SIRANE (Soulhac et al., 2011, 2012, 2017) uses a box model to determine pollutant concentrations in street canyons, assuming that concentrations are uniform along each street segment. SIRANE considers horizontal wind advection, mass transfer between streets at street intersections, turbulent vertical transfer between streets and the free atmosphere. Background concentrations above streets are calculated using a Gaussian plume distribution. The simplified parametrizations for airflow and mass transfer implemented in SIRANE are based on computational fluid dynamic simulations and wind tunnel experiments (Soulhac et al., 2008, 2009). The box model is applied to streets with an aspect ratio α_r higher than 0.3, with $\alpha_r = H/W$, H and W are the street height and width respectively (Landsberg, 1981). If α_r is lower than 0.3, the street is treated as an open terrain, and the concentrations are taken equal to background concentrations above the street, and they are simulated with a Gaussian plume model. However, estimating background concentrations above streets with a Gaussian plume model inhibits a comprehensive atmospheric chemistry treatment, impacting the modeling of secondary pollutant concentrations, such as O_3 and the secondary formation of NO_2 concentrations. Although SIRANE uses a stationary hypothesis for pollutant transport, a new version of SIRANE, named SIRANERISK (Soulhac et al., 2016), removes the steady state hypothesis and simulates dispersion above street canyons using a Gaussian puff model.

The Model of Urban Network of Intersecting Canyons and Highways (MUNICH)~~(Kim et al., 2018)~~ , developed by Kim et al. (2018), presents a similar box-model ~~parameterization~~ parametrization as SIRANE, but it does not employ a Gaussian model to determinate background concentrations. They may be provided by measurements, as in Kim et al. (2018), or regional-scale CTMs, as in our study. This approach allows the implementation of a comprehensive chemical module to better estimate secondary pollutant formation. MUNICH differentiates three types of street canyons: (i) narrow canyons with $\alpha_r > 2/3$, (ii) intermediate canyons with $1/3 \leq \alpha_r \leq 2/3$, and wide canyons (iii) with $\alpha_r < 1/3$. The aspect ratio α_r is used to determine the wind speed in the streets and the vertical mass transfer between the streets and the atmosphere.

Despite this large diversity of ~~parameterizations~~ parametrizations increasingly complex, local-scale models often assume that background concentrations are constant and/or use simplified chemistry. Although MUNICH is able to consider the temporal and spatial evolution of background concentrations, the coupling between the background and street concentrations is not ~~dynamic~~two-way, but one-way. In other words, the concentrations calculated in the streets do not influence the background concentrations. The coupling between background and street concentrations is ~~dynamic~~ two-way in the multi-scale Street-In-Grid (SinG) model (Kim et al., 2018), which couples the regional scale model Polair3D (Sartelet et al., 2007) to the street-network model MUNICH, using the Polyphemus platform (Mallet et al., 2007). The street-network model is coupled to the first vertical level of the regional scale model. At each time step, the mass transfer between the street and the atmosphere influences both background and street concentrations. Thus, SinG combines dynamically an advanced treatment of atmospheric transport and chemistry at the regional scale with a street-network parametrization formulated for streets with different aspect ratios. Kim et al. (2018) validated SinG over a street-network located at a Paris suburb, regarding NO_2, NO and NO_x concentrations. Compared to the street or to the regional model, the SinG multi-scale approach improved NO_2 and NO_x simulated concentrations compared to observations. However, the original version of MUNICH and SinG assume a stationary hypothesis to calculate

pollutant transport in streets. As shown later in this work, the stationary hypothesis impacts secondary pollutant formation and the concentrations of reactive species, such as NO_2.

The two-way dynamic coupling between 3D chemistry-transport and local-scale models started with modeling plumes from tall stacks, as described in Seigneur et al. (1983), Karamchandani et al. (2002), ~~Karamchandani et al. (2006), Morris et al. (2002b)and Morris et al. (2002a)~~ Morris et al. (2002b), Morris et al. (2002a) and Karamchandani et al. (2006). In all these studies, a dynamic interaction between local and regional scales is performed: the average grid concentration is used as background concentration to calculate plume dispersion, and the pollutant concentrations present in the plume are mixed to the grid concentrations depending on the plume characteristics. Different criteria are applied to define the moment where the pollutant concentrations of the plume are mixed to the grid concentrations. The criteria vary with the plume size and the mature plume stage (based on chemical reactions). Karamchandani et al. (2011) present an overview of sub-grid scale plume models, also named "Plume-in-Grid" (PinG) models. Over time, PinG models have been generalized to deal with different types of emission sources, such as linear and surface sources, allowing a more accurate modeling of dispersion around ship emissions and traffic emissions from roadways (Vijayaraghavan et al., 2006; Freitas et al., 2007; Vijayaraghavan et al., 2008; Cariolle et al., 2009; Briant and Seigneur, 2013; Rissman et al., 2013).

For streets, several models consider a multi-scale modeling between streets and background concentrations, although this multi-scale is most often not ~~dynamic~~two ways. Jensen et al. (2017) performed a high resolution multi-scale air-quality simulation for all streets in Denmark in 2012 using the model THOR (Brandt et al., 2001c, a, b), which combines three air-quality models at different spatial scales: ~~DEOM~~ DEHM (Danish Eulerian ~~Operational~~ Hemispheric Model), which provides regional background concentrations to UBM (Urban Background Scale Modeling), which then provides urban background concentrations to OSPM at the local scale. Comparisons between the annual average concentrations calculated with THOR and measured at air-quality stations show a fairly good agreement, especially for NO_2, whereas $PM_{2.5}$ and PM_{10} are underestimated. With this kind of ~~non-dynamic~~ one-way multi-scale modeling, traffic emissions are counted twice: they are input to the street model to estimate street concentrations, as well as to the regional model to estimate background concentrations. To avoid this double counting in multi-scale modeling, Stocker et al. (2012) used a ~~different approach : the~~ specific approach to couple the regional-scale model CMAQ and the local-scale Gaussian model ADMS-Urban~~is applied to estimate the initial dispersion of traffic emissions~~ . The local-scale effect of pollutant dispersion is calculated during a mixing time τ_m (typically ~~1 hour) . The multi-scale concentrations are obtained by subtracting the gridded concentrations simulated after this mixing time τ_m to the sum of the local-scale concentrations simulated with ADMS-Urban and the~~ 1h) by computing the differences in concentrations due to the dispersion of traffic emission using a Gaussian and a non-Gaussian approach on the spatial grid of CMAQ. Then the multi-scale concentrations are obtained by adding this local-scale effect to the CMAQ regional-scale concentrations. Hood et al. (2018) applied this model over London for 2012, using the regional-scale model EMEP4UK (Vieno et al., 2009), to simulate NO_2, NO_x, O_3, CO, $PM_{2.5}$ and PM_{10} concentrations. They showed that the multi-scale model improves NO_2 and particulate concentrations compared to the regional model, especially at near-road sites.

The objective of this work is to quantify the effect of a two-way dynamic multi-scale modeling between the regional and local scales on NO, NO_2 and NO_x concentrations over the street network of Paris city. To do so, SinG, MUNICH and Polair3D

simulated concentrations are compared. Different aspects related to model hypothesis and numerical parameters are studied: the impact of the stationary hypothesis often used for pollutant dispersion in streets and the ~~time step~~ time-step stability. Model validation is done by comparing simulated and observed concentrations at both traffic and urban background stations. The local, regional and multi-scale models MUNICH, Polair3D and SinG are presented in the ~~first~~ second section of this paper. The ~~second~~ third section describes the setup of the simulations over Paris city. The ~~third~~ fourth section studies the impact of the stationary hypothesis and the numerical stability of the multi-scale model. The ~~fourth~~ fifth section compares the simulated concentrations with air-quality measurements at traffic and background stations. Finally, the ~~fifth~~ sixth section studies the influence of the two-way dynamic coupling between the regional and local scales.

2 Model description

Street-in-Grid (SinG) is a multi-scale model that ~~acts as an interface between the 3D chemistry-transport model Polair3D and~~ couples the street-network ~~model MUNICH (~~Model of Urban Network of Intersecting Canyons and Highways ~~)~~(MUNICH) with the 3D chemistry-transport model Polair3D using a two-way dynamic multi-scale approach. MUNICH is coupled to the first vertical level of Polair3D and the mass transfer between the local and regional scales is computed at each time step of Polair3D. More details about the two-way dynamic coupling are described in the section 3 of Kim et al. (2018) and in the section 2.3 of this paper. This ~~dynamic (two ways)~~ two-way coupling presents several advantages compared to a one-way formulation, as: (i) concentrations at the local and regional scales affect each other; (ii) no double counting of emissions is performed; (iii) the chemical and physical parametrizations used at the local and regional scales are consistent: both scales use the same chemical module and meteorological data. But this approach also increases the computational time by a factor of about 1.28 (if MUNICH is not parallelized, as in the simulations performed here). The regional and local-scale model, Polair3D and MUNICH, are now described emphasizing the numerical parameters and assumptions investigated in this study.

2.1 Regional scale - Polair3D

Polair3D, as described in Boutahar et al. (2004) and Sartelet et al. (2007), is a 3D Eulerian model which solves numerically the chemistry-transport equation, considering advection, diffusion, dry and wet deposition processes and chemical transformations. Polair3D was used in many studies to simulate gas and particle concentrations at regional scale at different locations ~~,~~ (e.g., Royer et al. (2011), Sartelet et al. (2012), ~~Abdallah et al. (2018), including Greater Paris Sartelet et al. (2018), Zhu et al. (2016a), Zhu et al. (2016b)~~Couvidat et al. (2013), Kim et al. (2014), Kim et al. (2015), ~~Kim et al. (2014), Couvidat et al. (2013), Royer et al. (2011)~~Zhu et al. (2016a), Zhu et al. (2016b), Abdallah et al. (2018), Sartelet et al. (2018)).

Polair3D numerically solves the chemistry-transport equation by applying a first-order operator, splitting between transport and chemistry with the sequence: advection-diffusion-chemistry (Korsakissok et al., 2006). Pourchet et al. (2005) performed divers numerical tests with Polair3D. They showed that pollutant concentrations are not significantly influenced by the splitting method nor the splitting time step, if a splitting time step lower than 600 s is used at the continental scale.

2.2 Local scale - MUNICH

The Model of Urban Network of Intersecting Canyons and Highways (MUNICH) is a street-network box model formulated to calculate pollutant concentrations in street segments. It is composed of two main components: a street-canyon and an intersection components. A complete description of MUNICH may be found in Kim et al. (2018).

MUNICH assumes that the height and width of each street segment are constant, and that concentrations are uniform within the street segment. Because MUNICH is a stand-alone model, it does not have any constraint on street dimensions. However, in the SinG model, street height cannot be higher than the first vertical level of the regional-scale module. The time evolution of the mass ~~Q~~ M of pollutants in each street segment may be described by~~equation (1)~~:

$$\frac{dQ}{dt}\frac{dM}{dt} = \left.\frac{dQ}{dt}\frac{dM}{dt}\right|_{\text{transp}} + \left.\frac{dQ}{dt}\frac{dM}{dt}\right|_{\text{chem}} \tag{1}$$

$$\left.\frac{dQ}{dt}\frac{dM}{dt}\right|_{\text{transp}} = \underbrace{(Q_{inflow} + Q_{emis})}_{inlet\ flux} - \underbrace{(Q_{outflow} + Q_{vert} + Q_{dep})}_{outlet\ flux}, \tag{2}$$

where Q_{emis} represents the traffic mass emission ~~rate~~flux, Q_{inflow} the mass inflow ~~rate~~ flux at intersections, Q_{vert} the turbulent mass flux ~~rate~~ between the atmosphere and the street, $Q_{outflow}$ the outflow flux, and Q_{dep} the deposition ~~flow; each of this~~ flux; each term is detailed in Kim et al. (2018). According to Kim et al. (2018), $Q_{outflow}$ is calculated based on outflow air flux (function of street dimensions, horizontal wind speed) and street concentrations. Q_{dep} depends on deposition rates, and both terms are calculated following equations (3) and (5):

$$Q_{outflow} = Q_{air} C_{st}; \text{ with } Q_{air} = HWu_{st}, \tag{3}$$

with

$$Q_{air} = HWu_{st} \tag{4}$$

where ~~H and W~~ Q_{air} is the air flow, C_{st} the pollutant concentration in the street, H and W are the street height and width, and u_{st} is the mean air velocity in the street,

$$Q_{dep} = F_{dep} C_{st} \tag{5}$$

where F_{dep} is the deposition ~~flow~~rate.

According to the equation (8) of Kim et al. (2018) and equation (8) of this paper, Q_{vert} is inversely proportional to the aspect ratio α_r of the street. Therefore, the vertical mass transfer is more significant for wide streets than for street canyons.

The aspect ratio α_r is also used to determine the wind speed in the streets, as described in equations (9), (10) and (11) of Kim et al. (2018).

MUNICH uses a first order splitting scheme between transport and chemistry to solve equation (1).

In the work of Kim et al. (2018), the splitting time step is fixed (100 s) and the time evolution of the mass of pollutants due to transport is computed at each time step using a stationary hypothesis:

$$\left.\frac{dQ}{dt}\frac{dM}{dt}\right|_{\text{transp}} = 0, \tag{6}$$

which leads to the following expressions for the street concentrations C_{st}:

$$C_{st} = \frac{Q_{emis} + Q_{inflow} + \gamma C_{bg}}{\gamma + Q_{air} + F_{dep}}, \tag{7}$$

where γ ~~defines the transfer rate~~ is related to the transfer flux Q_{vert} between the street and the background concentration C_{bg}:

$$Q_{vert} = \gamma\,(C_{st} - C_{bg}) \quad \text{with } \gamma = \beta\sigma_w W L \frac{1}{1+\alpha_r} \tag{8}$$

defined as

$$\gamma = \beta\sigma_w W L \frac{1}{1+\alpha_r} \tag{9}$$

with β a constant equal to 0.45, σ_w the standard deviation of the vertical wind speed, which are calculated depending on the atmospheric stability (Soulhac et al., 2011), and W and L the width and length of the street.

The time evolution of the concentrations of ~~pollutants~~ of gases due to chemistry is then computed using the chemical ~~module~~ mechanism CB05 (Yarwood et al., 2005), and the Rosenbrock solver (Rosenbrock, 1963; Sandu et al., 1997).

In this study, a new algorithm is defined to calculate pollutant concentrations in streets without the stationary assumption. The non-stationary calculation of pollutant concentrations in streets solves equation (1) using an explicit two-stage Runge-Kutta method: the explicit trapezoidal rule of order 2 (ETR) ~~, as~~ (Ascher and Petzold, 1998), also detailed in Sartelet et al. (2006). The choice of the initial time step and the time-step adjustment during the simulations are done depending on the evolution of the concentrations due to transport-related processes:

$$\begin{aligned} C^{n+1} &\equiv C^n + \frac{\Delta t}{2}\left[F(C^n) + F(C^*)\right] \\ C^* &\equiv C^n + \Delta t\, F(C^n) \end{aligned}$$

$$C^{n+1} = C^n + \frac{\Delta t}{2}\left[F(C^n) + F(C^*)\right] \tag{10}$$

$$C^* = C^n + \Delta t\, F(C^n) \tag{11}$$

where C^n is the concentration at time t^n, $F(C^n)$ represents the time derivative of C^n due to transport-related processes and is obtained by equation (2). After each time step Δt, the time step is adjusted:

$$\Delta t^{n+1} = \Delta t \frac{\Delta_0}{\Delta_1} \text{ with } \Delta_1 = \frac{C^{n+1} - C^*}{C^*}_2 \cdot \sqrt[n]{\frac{\Delta_0}{\Delta_1}} \tag{12}$$

where

$$\Delta_1 = \left|\left| \frac{C^{n+1} - C^*}{C^{n+1}} \right|\right|_2 . \tag{13}$$

with Δ_0 the relative error precision equals 0.01.

Because chemical reactions are represented by a stiff set of equations with fast radical chemistry, chemistry processes are solved after transport processes over the time step defined by the ETR algorithm. Note that as in the regional-scale model, chemistry processes are solved with the Rosenbrock algorithm ~~(Voss and Khaliq, 2001)~~ using time steps that may be smaller than the splitting time step defined by the ETR algorithm.

2.3 Street-in-Grid model (SinG)

SinG interconnects regional and local scales at each time step. Pollutant concentrations are calculated in streets at the local scale, and they are transferred to the regional scale with a vertical mass flux (see equation (8)) between the street and the regional background concentrations of the first vertical grid level of the CTM. The vertical mass flux corresponds to an emission term for the regional-scale model, and it is used in the local-scale model to compute the time evolution of street concentrations as ~~details~~ detailed in equation (2).

Note that the background concentrations used in equation (8) to compute the vertical mass flux are not exactly those computed by the regional-scale model. Because it does not consider buildings, the volume of the cell in which the concentrations are computed with the regional-scale model is actually larger than the volume of the cell if buildings are considered. Therefore, for each cell i of the regional model, the background ~~concentration~~ concentrations over the canopy $C^i_{bg,cor}$ are obtained from regional-scale concentrations corrected to take into account the presence of buildings:

$$C^i_{bg,cor} = \frac{V^i_{cell}}{(V^i_{cell} - V^i_{build})} C^i_{bg}, \tag{14}$$

where V^i_{build} is the buildings volume, V^i_{cell} is the grid cell volume, and C^i_{bg} is the background concentration calculated over the whole cell volume V^i_{cell} with the regional-scale model.

At each grid cell i, SinG performs an average between the pollutant mass in streets (Q^i_{st}) and the background pollutant mass (Q^i_{bg}) to calculate output concentrations at the regional scale (C^i_{reg}), as:

$$C^i_{reg} = \frac{Q^i_{st} + Q^i_{bg}}{V_{cell}} \text{ with } Q_{st} = \sum_{st\ in\ the\ cell} C^i_{st} V_{st} \text{ and } Q^i_{bg} = C^i_{bg} V_{cell}.$$

2.4 ~~Setup of air-quality simulations over Paris city~~

$$C^i_{reg} = \frac{Q^i_{st} + Q^i_{bg}}{V_{cell}}, \tag{15}$$

$$Q_{st} = \sum_{st\ in\ the\ cell} C^i_{st} V_{st}, \tag{16}$$

$$Q^i_{bg} = C^i_{bg} V_{cell}. \tag{17}$$

3 Setup of air-quality simulations over Paris city

This ~~sections~~ section describes the model configuration as well as the input data used for the regional and local-scale simulations. All simulations are performed from the 1^{st} to 28^{th} May 2014, with a spin-up of two days.

3.1 Setup ~~for~~ of regional-scale simulations

~~SinG~~ The two-way SinG model is applied over Paris city (domain 4), using a spatial resolution of 1 km $\times$ 1 km. Initial and boundary conditions are obtained from one-way nesting simulations using Polair3D over three additional simulations covering Europe (domain 1), France (domain 2) and Île-de-France region (domain 3). The spatial resolution for those simulations is 45 km $\times$ 45 km, 9 km $\times$ 9 km and 3 km $\times$ 3 km, respectively. Figure 1 illustrates the different domains, with domain 4 corresponding to the Paris city domain. The four nested simulations over the domains shown in Figure 1 use the same vertical discretization with 14 levels between 0 and ~~12000 m~~12 km, represented in Figure 2.

The initial and boundary conditions of the largest domain (over Europe) are obtained from a global-scale chemical-transport simulation using MOZART-4 (model for Ozone and Related Chemical Tracers) (Emmons et al., 2010) coupled to the aerosol module GEOS-5 (Goddard Earth Observing System Model) (Chin et al., 2002). The spatial resolution of the MOZART-4/GEOS-5 simulation is 1.9° $\times$ 2.5°, with 56 vertical levels.

Meteorological data for the four domains are calculated by the ~~WRF model (~~Weather Research and Forecasting ~~) (Skamarock et al., 2008)~~ version 3.9.1.1 with a two-way nesting (Skamarock et al., 2008), employing the same spatial resolutions as used in Polair3D nesting simulations (45 km $\times$ 45 km, 9 km $\times$ 9 km, 3 km $\times$ 3 km and 1 km $\times$ 1 km for domains 4 to 1 respectively), with

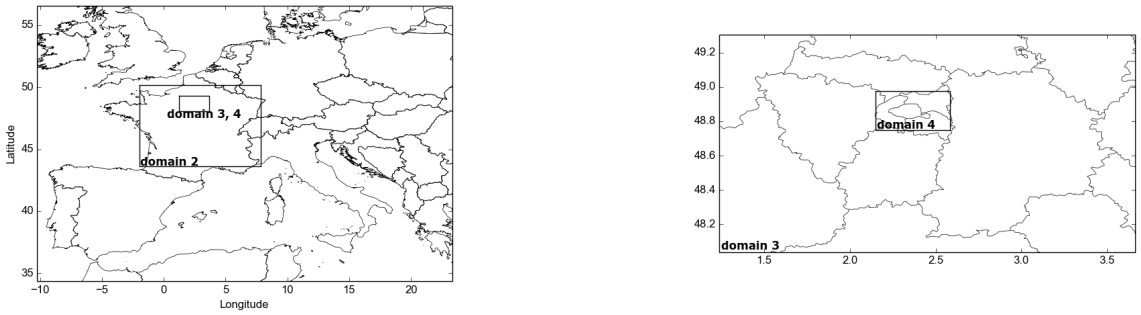

Figure 1. Domains simulated: Europe (domain 1), France (domain 2), Île de France region (domain 3), and Paris city (domain 4).

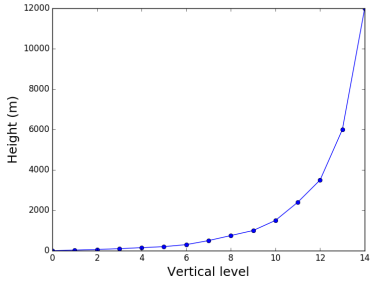

Figure 2. Vertical levels ~~employed~~ used in all regional-scale simulations.

38 vertical levels, from 0 to ~~5000 m~~21 km. Observational data of wind speed, wind direction, pressure and temperature from Paris Orly meteorological station are used as input data for the simulations over Paris city (domain 4) using the nudging point technique. WRF domains are represented in Figure 3, and Table 1 indicates the main physical ~~and chemical~~ options employed in WRF simulations.

Table 1. Main physical options used in WRF simulations

mp_physics	microphysics	WSM 6-class graupel scheme
cu_physics	cumulus	Kain-Fritsch (new Eta) scheme
ra_lw_physics	longwave radiation	RRTM scheme: Rapid Radiative Transfer Model
ra_sw_physics	shortwave radiation	Dudhia scheme
bl_pbl_physics	boundary-layer	MYNN 2.5 level TKE scheme
sf_sfclay_physics	surface-layer	MYNNSFC
sf_surface_physics	land-surface	Noah Land-Surface Model

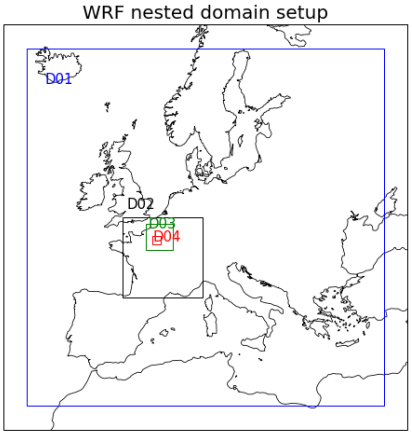

Figure 3. ~~Domains simulated~~ Simulated domains using WRF: Europe (D01), France (D02), Île-de-France region (D03), and Paris city (D04).

Dry-deposition velocities of gas species are estimated following Zhang et al. (2003), and below-cloud scavenging following Sportisse and Du Bois (2002), see Sartelet et al. (2007) for more details on the deposition schemes used. Biogenic emissions over all domains are estimated using the Model of Emissions of Gases and Aerosols from Nature (MEGAN v2.04). Concerning anthropogenic emissions, over the domains 1, 2 and outside Île-de-France over the domain 3, they are calculated using EMEP (European Monitoring and Evaluation Program) emission inventory for the year 2014, with a spatial resolution of $0.1° \times 0.1°$. Over Île-de-France of the domain 3 and over the domain 4, they are calculated using the emission inventory of 2012, provided by the air-quality agency of Paris (AIRPARIF). For traffic emissions, AIRPARIF used the HEAVEN bottom-up traffic emissions model (https://trimis.ec.europa.eu/~~sites/default/files/~~project/~~documents/20090917_162316_73833_HEAVEN%20-%20Final%20Report.pd~~ with fleet and technology data specific of 2013 and 2014. Anthropogenic emissions followed the vertical distribution defined by Bieser et al. (2011) for the different activity sectors. More details on emission data and speciations may be found in Sartelet et al. (2018).

Note that in SinG, traffic emissions are only considered at the local scale and not at the regional scale to avoid double counting of emissions, as shown in Figure 4.

3.2 Setup ~~for~~ of local-scale simulations

The street network used in this study was provided by AIRPARIF. It contains the main streets of Paris city, totalizing 3819 streets. Apart from the location and length of the street segments, the streets' average dimensions (height and width) need to be defined.

A processing tool was developed to treat three different databases to determine street dimensions. The streets' widths are computed by summing the pavement width (from the BDTOPO database, available at http://professionnels.ign.fr/bdtopo) and

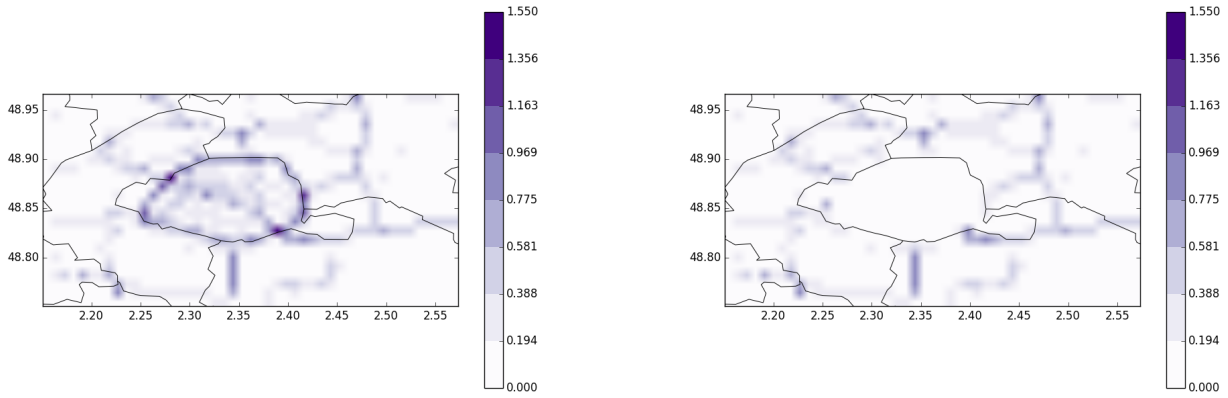

Figure 4. ~~For~~ Average over the ~~Paris simulations using Polair3D and SinG, average anthropogenic emissions~~ simulated period of NO_2 anthropogenic emissions [μg.s^{-1}.m^{-2}] used as input of the regional-scale ~~simulation~~ simulations over Paris city with Polair3D (left panel), and as input of the regional-scale module of the multi-scale ~~simulation~~ simulations with SinG (right panel).

the two sidewalk widths (from an opensource public database "opendataparis", available at https://www.data.gouv.fr/fr/datasets/trottoirs-des-rues-de-paris-prs/). The streets' heights are determined using the Parisian urban planning agency (APUR) database (https://www.apur.or The average height adopted at each street is calculated considering the mean height of all buildings located near the street axis, with a maximal distance of 10 m.

For the validity of the MUNICH model, buildings' heights cannot be higher than the first vertical level of the regional model, so a maximum height of 30 m is adopted in this study. This limitation is acceptable over Paris, because the average height of buildings is about 15 m. A minimum street width equal to 10 m is adopted over the whole domain, imposing 10 m width to very narrow streets.

A few street segments in the domain, especially along the ring road around Paris ("boulevard périphérique") are tunnels. For those segments, traffic emissions are not assigned to the segment itself, but to two "virtual" streets added at each tunnel extremity, with half of the tunnel emissions each. The width of these virtual streets is the same as the width of the tunnel, and an arbitrary length of 3 m is chosen.

As Paris has an important number of public parks and gardens, the average vegetation height is also considered for streets along these areas, and the model considers that the street's height is the average height of buildings and trees. The average trees' height is estimated to be about 13 m, considering the whole domain. It is calculated using a database containing the height of all trees in public spaces of Paris, available online "opendataparis" (https://opendata.paris.fr/explore/dataset/les-arbres/information/).

The street network and the street characteristics are used for the local-scale simulations using MUNICH and SinG, where wind profile and turbulent exchange depend on the aspect ratio α_r (as mentioned in section 2.2) of the streets. Table 2 indicates the maximum, average, and minimum street dimensions of the whole street-network used in this study.

Table 2. Maximum, average, and minimum street dimensions of the whole street-network used in this study

	Length (m)	Height (m)	Width (m)
Average	179.3	15.8	18.5
Minimum	3.0	5.0	10.0
Maximum	1096.8	30.0	77.9

Emission data over the street segments is provided by AIRPARIF using the HEAVEN model (see Sartelet et al. (2018)). Figure 5 illustrates the average emissions of NO_2 during ~~all~~ the simulation period. The ~~most important~~ highest emissions are located along the ring road ("boulevard périphérique"), as expected. This zone presents the most important road traffic in Paris city.

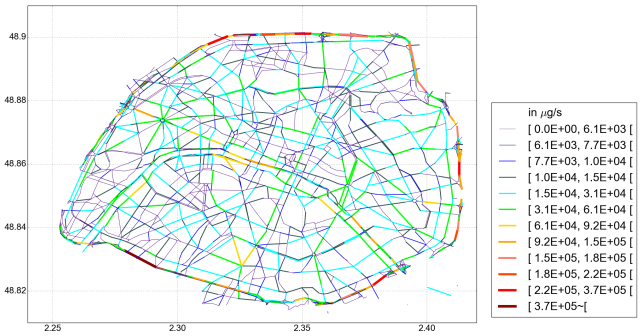

Figure 5. Average traffic emissions of NO_2 [$\mu g.s^{-1}$] calculated for local-scale simulations

Meteorological data for each street and intersection are obtained from the WRF simulations, as in the regional-scale simulation over Paris city. MUNICH simulations also require background concentrations as input data. They are obtained from ~~a~~ Polair3D ~~simulation~~ simulations over the Paris city regional-scale domain. Note that the Polair3D ~~simulation uses~~ simulations use all emissions, including traffic, as input data (as indicated in Figure 4), and that Polair3D, SinG and MUNICH simulations are performed using the same temporal resolution.

3.3 List of simulations

Different numerical simulations are performed in order to compare the concentrations computed by SinG and MUNICH, as listed bellow. Numerical parameters (main time step) and model hypothesis (stationary hypothesis or not) are analyzed. The main time step corresponds to the splitting time step between transport and chemistry in the regional-scale chemistry-transport

model Polair3D. As in Polair3D, in MUNICH and SinG, the main time step corresponds to the time step used to split local-scale transport and chemistry if the stationary hypothesis is used. If the stationary hypothesis is not made, then the splitting time step between local-scale transport and chemistry is estimated and adjusted as detailed in section 2.2. In SinG, the main time step also corresponds to the splitting time step between the regional-scale (Polair3D) and local-scale (MUNICH) modules. Different simulations are conducted with a main time step equal to 100 s or 600 s, and with or without the stationary hypothesis in MUNICH and SinG, as detailed in Table 3.

Sim. number	Model	time step	Stat. hyp.
1	MUNICH	600 s	yes
2	MUNICH	100 s	yes
3	MUNICH	600 s	no
4	MUNICH	100 s	no
5	SinG	600 s	yes
6	SinG	100 s	yes
7	SinG	600 s	no
8	SinG	100 s	no

Table 3. List of the sensitivity simulations performed.

Simulated concentrations are compared with air-quality measurements at traffic and urban background stations. Figure 6 represents the street network emissions used in this study ~~,~~ (see section 3.2), also displaying the regional-scale grid mesh and the position of all stations considered. Air-quality stations comprise 5 urban stations (indicated by PA04C, PA07, PA12, PA13 PA18, with blue dots), and 8 traffic stations (BONAP, ELYS, HAUSS, CELES, BASCH, OPERA, SOULT and BP_EST~~).~~, with red dots).

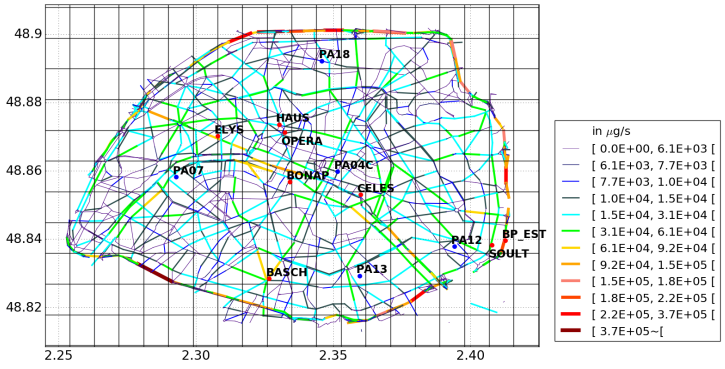

Figure 6. Street network with the regional-scale grid mesh and the position of the measurement stations.

4 Numerical stability and influence of the stationary hypothesis

As mentioned in section 3.3, different simulations with MUNICH and SinG are performed with different time steps, considering or not the stationary hypothesis. Figures ~~?? and ??~~ 7 and 8 represent the time evolution of average daily concentrations of NO_x, NO_2 and NO during the simulation period, as simulated with MUNICH and SinG, at ~~BONAP and CELES stations respectively~~CELES station. NO_x concentrations are independent of whether the stationary hypothesis is made or not, and of the choice of the main time step. However, in both MUNICH and SinG, street concentrations of NO_2 and NO are highly dependent on the choice of the time step when the stationary ~~hypothesis is made. This time-step dependency is observed using both MUNICH and SinG~~approach is used. This problem is solved with the non-stationary simulations, where street concentrations of NO_2 and NO are numerically stable and independent of the choice of the main time step. ~~Besides the numerical stability,~~ For example, regarding the concentrations simulated at CELES station by MUNICH with the stationary approach, the modification of the time step from 600s to 100s decreased by 5% NO_2 ~~and NO average concentrationsobtained using~~ concentrations and increased by 12% NO concentrations. With the non-stationary approach~~are closer to observations than those using the stationary hypothesis, as indicated in Table ??~~, these differences reduced to 0.1% for NO_2 concentrations and 0.2% for NO concentrations. Note that there are differences in the background concentrations of the regional-scale model if a time step of 600 s is used rather than 100 s. This explains the small differences on NO_2 concentrations observed at CELES station in Figure 8 using SinG with two different time steps (100 s and 600 s) and the non-stationary approach. Therefore, in the rest of this paper only the simulations performed with the non-stationary approach and a main time step of 100 ~~-~~s are analyzed.

~~Observations SinG non-stat. SinG stat.~~ Besides the numerical stability, NO_2 ~~55.80 64.03 85.59 NO 49.58 51.57 37.46~~

~~Observations SinG non-stat. SinG stat.~~ and NO average concentrations simulated using the non-stationary approach are closer to observations than those simulated using the stationary approach, as shown in Figures 7 and 8. The fraction bias of daily-average concentrations calculated with SinG (with a 100 s time-step) at CELES station is as high as 53% and -24% for NO_2 ~~46.24 54.34 61.14 NO 43.76 25.00 20.62~~ and NO respectively using the stationary approach, and it is reduced to 13% and 4% respectively using the non-stationary approach.

5 Comparisons to air-quality measurements

This section presents the comparisons between the measured concentrations of NO, NO_2 and NO_x and those simulated with MUNICH, Polair3D and SinG. As mentioned in section 3.3, air-quality stations comprise eight traffic stations and five urban stations. The criteria applied to evaluate the comparisons are the statistics detailed in Hanna and Chang (2012) and Herring and Huq (2018): $-0.3 < FB < 0.3$; $0.7 < MG < 1.3$; $NMSE < 3$; $VG < 1.6$; $FAC2 \geq 0.5$; $NAD < 0.3$. Hanna and Chang (2012) and Herring and Huq (2018) also defined a less strict criteria to be applied to urban areas: $-0.67 < FB < 0.67$; $NMSE < 6$; $FAC2 \geq 0.3$; $NAD < 0.5$. The definitions of these statistics are given in ~~Annexe~~Annex A1.

The statistics of the 3 models (Polair3D, MUNICH, SinG) for NO_2 and NO_x at traffic and background stations are indicated in Tables 4 and 5 respectively.

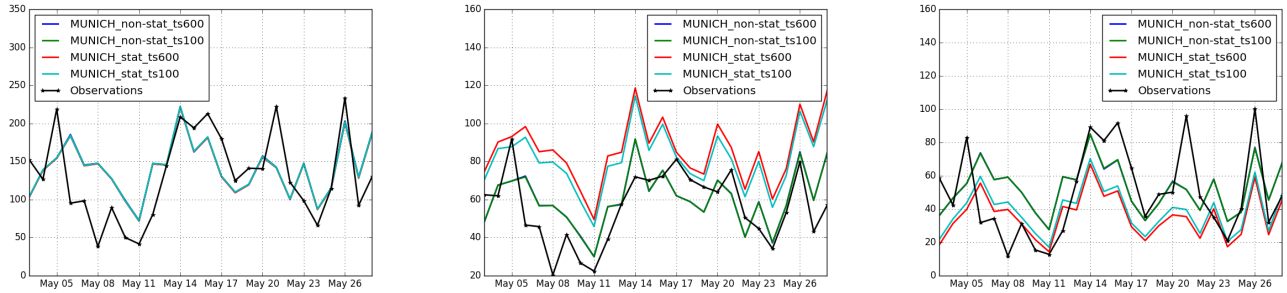

Figure 7. Daily-average concentrations of NO_x (left panel), NO_2 (middle panel), and NO (right panel) concentrations [$\mu g.m^{-3}$] calculated by MUNICH at CELES station with different main time steps, using the stationary and non-stationary approaches.

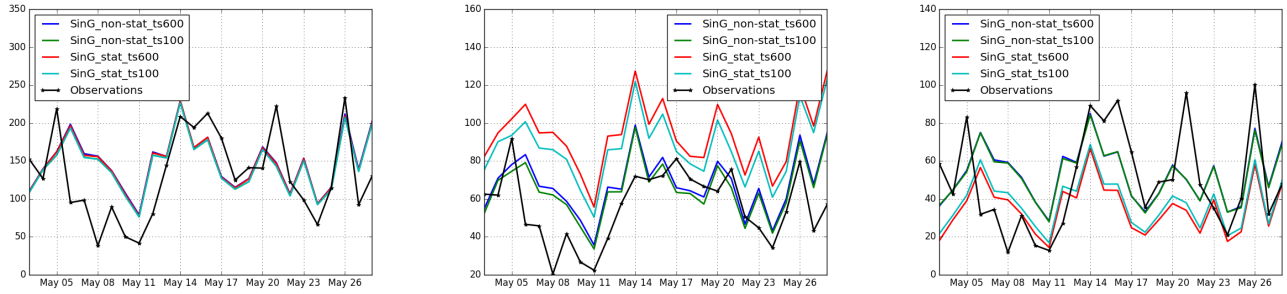

Figure 8. Daily-average concentrations of NO_x (left panel), NO_2 (middle panel), and NO (right panel) concentrations [$\mu g.m^{-3}$] calculated by SinG at ~~BONAP~~ CELES station with different main time steps, using the stationary and non-stationary approaches.

Table 4. Statistics at traffic stations (o and s represent the average observed and simulated concentrations respectively, in $\mu g.m^{-3}$).

	NO_2								**NO_x**							
	o	s	FB	MG	NMSE	VG	FAC2	NAD	o	s	FB	MG	NMSE	VG	FAC2	NAD
Polair3D	59.1	21.9	-0.88	0.39	1.26	3.21	0.20	0.44	146.4	27.7	-1.30	0.22	4.16	33.18	0.06	0.64
MUNICH	59.1	55.2	-0.06	0.97	0.12	1.15	0.94	0.14	146.4	108.8	-0.28	0.83	0.34	1.48	0.75	0.22
SinG	59.1	57.7	-0.01	1.02	0.11	1.14	0.94	0.13	146.4	109.5	-0.26	0.84	0.33	1.48	0.74	0.22

5.1 Traffic stations

As expected, Polair3D strongly underestimates NO_2 and NO_x concentrations at traffic stations, as shown by the statistical indicators of Table 4, and the performance criteria are not respected. However, NO_2 and NO_x concentrations are well modeled using both MUNICH and SinG.

Table 5. Statistics at background stations (o and s represent the average observed and simulated concentrations respectively, in μg.m^{-3}).

	NO_2								NO_x							
	o	s	FB	MG	NMSE	VG	FAC2	NAD	o	s	FB	MG	NMSE	VG	FAC2	NAD
Polair3D	31.0	21.2	-0.38	0.70	0.23	1.23	0.80	0.20	38.7	28.1	-0.37	0.72	0.26	1.23	0.81	0.20
SinG	31.0	23.3	-0.29	0.77	0.16	1.16	0.85	0.16	38.7	30.3	-0.25	0.82	0.17	1.15	0.83	0.15

As shown in Table 4, both MUNICH and SinG present similar statistics at the local scale, respecting the most strict performance criteria determined by Hanna and Chang (2012) for NO_2 and NO_x. Compared to MUNICH, the multi-scale approach of SinG improves the average statistical parameters for both pollutants.

The statistics at each station (see ~~Annexe~~Annex A2) show that the less strict criteria of Hanna and Chang (2012) indicated for urban areas are satisfied at all stations for NO_2 concentrations using MUNICH and SinG. The most strict criteria are even respected at all stations except BASCH. In both MUNICH and SinG simulations, NO concentrations tend to be underestimated, although the performance criteria are verified at 6 out of 8 stations. This underestimation may be due to the short life time of NO, leading to high uncertainties on dispersion, and questioning the assumption of uniform concentrations in streets. The NO underestimation is the most significant at stations located in big squares (OPERA and BASCH), indicating that the air flow ~~parameterization~~ parametrization for big squares may need to be improved. Note that because of the underestimation of NO concentrations at OPERA and BASCH, the performance criteria for NO_x are not respected at BASCH and only the less strict performance criteria are respected at OPERA.

The daily evolution of NO_x, NO_2 and NO concentrations is well simulated, as shown in Figures 9 and 10, which display the time evolution of daily concentrations of NO_x, NO_2 and NO simulated with MUNICH, SinG and Polair3D at CELES and SOULT stations. However, NO_2 concentrations are overestimated at almost all stations from the 9^{th} to the 11^{th} May. This period corresponds to a french holiday, suggesting that the temporal variability of emissions needs to be modified in the model for those days. Beyond daily average concentrations, both SinG and MUNICH represent well the time evolution of hourly concentrations, as shown in Figure 11. The better agreement of SinG and MUNICH during the morning peak than the evening one may be due to difficulties in modeling the atmospheric boundary height in the evening, and to higher day-to-day variability of traffic emissions in the evening than in the morning.

Table 6 indicates the average values of air-quality measurements and SinG concentrations, and the corresponding ratios of NO_2/NO. The ratios are overestimated in the simulations: they vary between 0.80 and 2.06 in the measurements, and between 0.98 and 2.80 in the simulations. The ratios are well simulated at CELES, SOULT and BP_EST stations, which are located in streets with high traffic emissions. However, they are ~~strongly~~ overestimated at other stations, such as those in big squares (OPERA, BASCH). This may be due to the short life time of NO, for which the assumption of uniform concentrations in wide streets and big squares may not be verified.

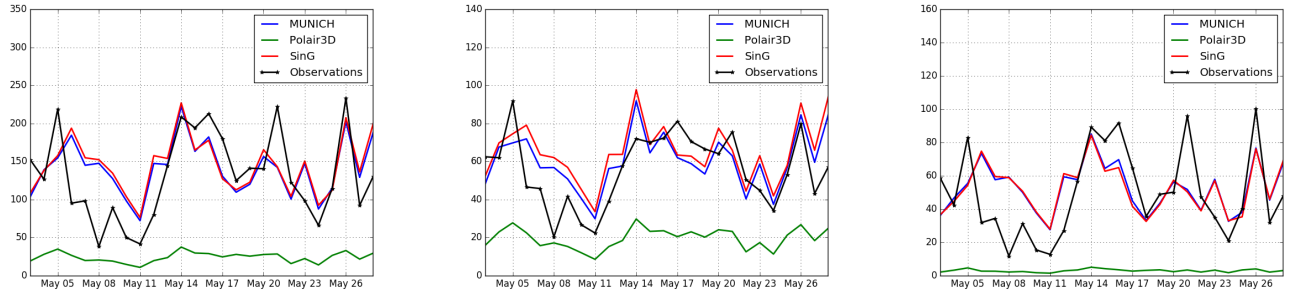

Figure 9. Daily-average NO_x (left panel), NO_2 (middle panel) and NO (right panel) concentrations [$\mu g.m^{-3}$] observed and simulated at CELES station with MUNICH, SinG and Polair3D.

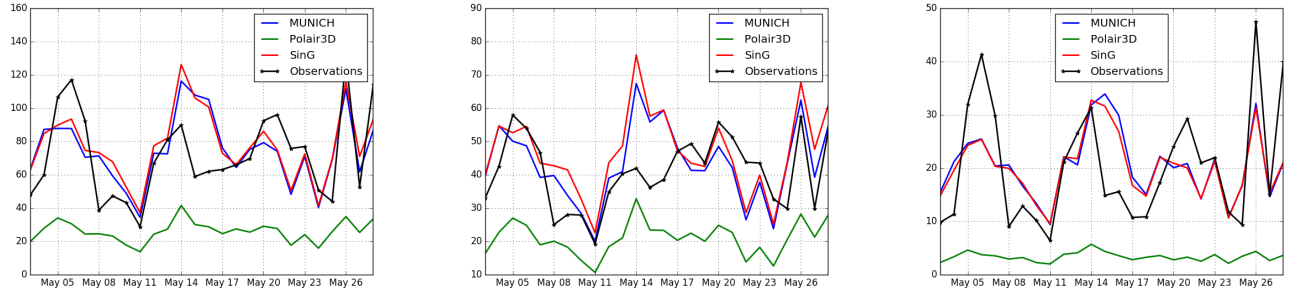

Figure 10. Daily-average NO_x (left panel), NO_2 (middle panel) and NO (right panel) concentrations [$\mu g.m^{-3}$] observed and simulated at SOULT station with MUNICH, SinG and Polair3D.

5.2 Background stations

Although both SinG and Polair3D perform well at simulating background NO_2 and NO_x concentrations, the multi-scale approach SinG improves the statistics of comparisons to measurements at urban background stations. Table 5 presents the statistics at urban background stations for the NO_2 and NO_x concentrations simulated with Polair3D and SinG. The multi-scale approach used in SinG improved all statistical parameters, especially the fractional bias, for both NO_2 and ~~NO~~NO_x. Regarding the simulated period, SinG respects the most strict performance criteria defined by Hanna and Chang (2012).

As expected, the differences between NO_x concentrations simulated with SinG and Polair3D are the highest at stations where vehicular traffic is high. Figures 12 and 13 show the time-evolution of daily NO, NO_2 and NO_x concentrations at the background stations PA04C and PA13. PA04C is a station located nearby an important traffic area, while PA13 is located in an

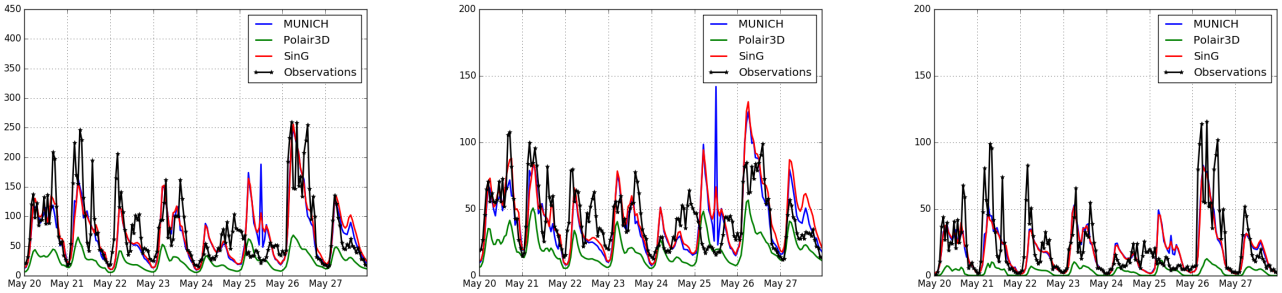

Figure 11. Hourly-average NO_x (left panel), NO_2 (middle panel) and NO (right panel) concentrations [$\mu g.m^{-3}$] observed and simulated at SOULT station with MUNICH, SinG and Polair3D.

Table 6. Average concentrations measured and simulated with SinG of NO_x, NO_2, NO and NO_2/NO ratios at traffic stations (o and s represent the observed and simulated average respectively, in $\mu g.m^{-3}$).

			NO_2		**NO**		**NO_x**		**NO_2/NO**	
	Adjacent to big squares	High emissions	o	s	o	s	o	s	o	s
CELES	no	yes	55.8	64.0	49.6	51.6	131.5	143.1	1.12	1.24
BONAP	no	no	46.2	54.3	43.7	25.0	113.1	92.7	1.06	2.17
SOULT	no	yes	40.4	46.1	19.6	20.1	70.3	77.0	2.06	2.29
ELYS	yes	yes	51.0	49.8	38.4	18.5	109.8	78.1	1.33	2.69
OPERA	yes	yes	74.3	60.3	81.1	27.7	198.5	102.8	0.92	2.17
HAUS	no	no	56.1	55.5	37.2	19.8	112.8	86.0	1.51	2.80
BP_EST	no	yes	70.8	80.3	88.6	81.5	206.3	205.2	0.80	0.98
BASCH	yes	yes	78.4	51.5	98.1	25.7	228.9	90.9	0.80	2.00

area with lower vehicle flux. SinG and Polair3D differences are more important at PA04C station than at PA13 station. More details about the differences of Polair3D and SinG concentrations are described in section 6.2.

Even though both SinG and Polair3D represent both well the measured background concentrations, the ~~dynamic~~ two-way coupling between spatial scales in SinG improves the ~~modelling~~ modeling of NO_2, NO and NO_x background concentrations. Furthermore, SinG proved to represent well NO_2 and NO_x concentrations both at local (traffic stations) and regional (background stations) scales.

6 Influence of the two-way dynamic coupling between the regional and local scales

This section analyzes the influence of the two-way dynamic coupling between the regional and local scales on NO, NO_2 and NO_x concentrations. This influence is analyzed by comparing the concentrations simulated with SinG and MUNICH at the

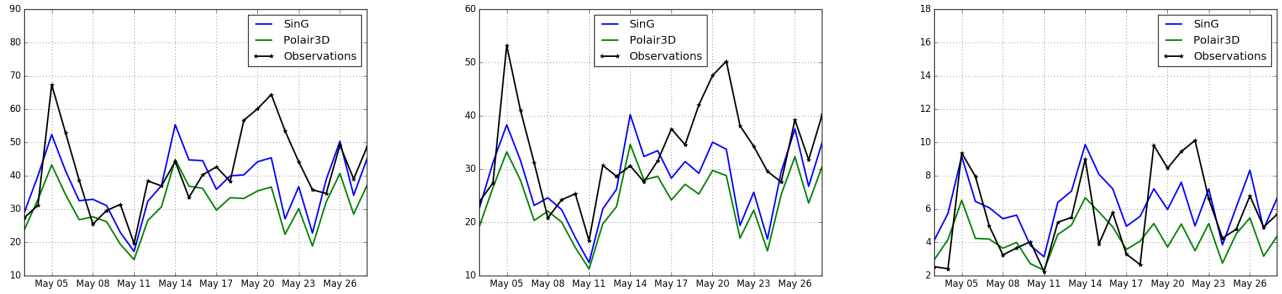

Figure 12. ~~Daily~~ Daily-average concentrations of NO_x (left panel), NO_2 (middle panel) and NO (right panel) [$\mu g.m^{-3}$] observed and simulated at PA04C station with SinG and Polair3D.

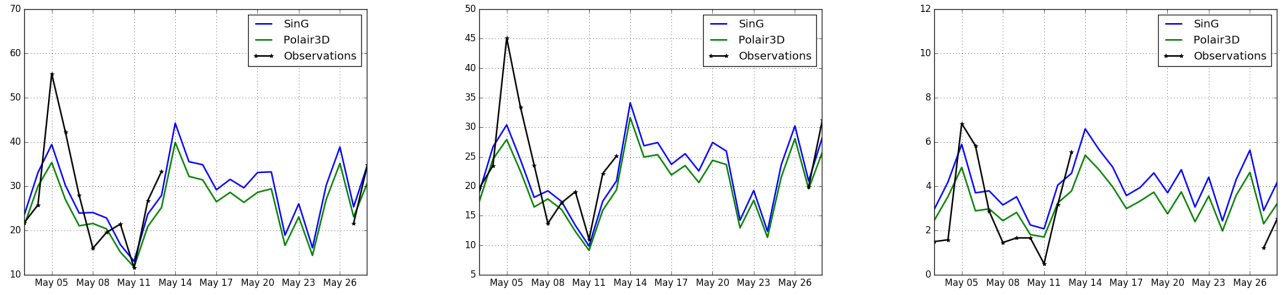

Figure 13. ~~Daily~~ Daily-average concentrations of NO_x (left panel), NO_2 (middle panel) and NO (right panel) [$\mu g.m^{-3}$] observed and simulated at PA13 station with SinG and Polair3D.

local scale (in streets), and SinG and Polair3D at the regional scale (background concentrations). The influence of different factors influencing this coupling is evaluated: the geometric characteristics of the streets, the inlet and output mass fluxes in the streets and the intensity of traffic emissions.

At both the regional and local scales, the larger differences between coupled and non-coupled simulations are observed in high traffic ~~emissions~~ emission areas. In these areas the vertical mass transfer between the local and regional scales tend to be more important for two main reasons: (i) the gradient between ~~street and~~ the street and the background concentrations is larger when traffic emissions are higher (see equation 8), and (ii) higher traffic emissions lead to higher influence of the mass advection flux between streets by mean wind, and therefore higher influence of vertical mass transfer at street intersections. If the vertical mass transfer is high, then the background concentrations may be higher in the two-way approach of SinG than in the one-way approach of MUNICH, leading to higher concentrations in streets. Figure 14 represents the mean relative differences between NO_2 concentrations simulated using coupled and non-coupled simulations at local (differences between

SinG and MUNICH) and regional scales (differences between SinG and Polair3D), averaged over the simulation period. In average, these mean relative differences are about 7.5% at the local scale and 11.3% at the regional scale.

To compute these relative differences, MUNICH and Polair3D concentrations were adopted as reference concentrations at the local and regional scales, respectively. The influence of dynamic coupling is now studied in more details, first at the local scale (in streets), and then at the regional scale.

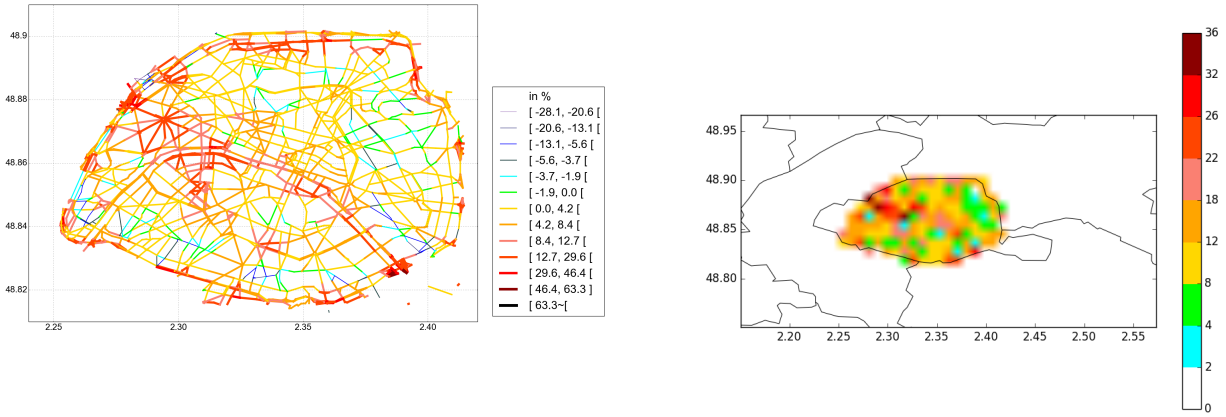

Figure 14. Relative differences (in %) between NO_2 concentrations simulated by SinG and MUNICH at the local scale (left panel) and by SinG and Polair3D at the regional scale (right panel).

6.1 Local scale

The differences between SinG and MUNICH are first analyzed at traffic stations. In SinG, the coupling depends on the concentration gradients between the street and the background, but also on the street dimensions, the standard deviation of vertical wind speed, and input/output mass fluxes at intersections. Table 7 summarizes the street characteristics, with L the street length, α_r the street aspect ratio, and NO_2 diff$(\%)_{s,m}$ the mean relative difference between NO_2 concentrations simulated with SinG and MUNICH over the simulation period. The differences between SinG and MUNICH concentrations are quite low: they are lower than 12% at each of the 8 traffic stations. In agreement with section 5.1 and Table 4, NO_2 concentrations simulated with SinG tend to be larger than those simulated with MUNICH, because the background concentrations in SinG are influenced by the high NO_x concentrations of the street network.

As explained in section 2.3, SinG transfers the vertical mass flux from streets and intersections to the regional scale to correct background concentrations. Therefore, the differences between MUNICH and SinG simulations are mostly due to differences in background concentrations. The time variations of the differences are illustrated in Figure 15, which represents the time evolution at CELES station of NO_2 concentrations in the streets and the background using MUNICH and SinG. The differences between the street and the background concentrations are strongly correlated. Higher are the differences between

Table 7. Street length (L), aspect ratio (α_r), number of connected streets, and the correspondent relative difference of NO_2 concentrations calculated by SinG and MUNICH at each traffic station.

Station	L (m)	α_r	Connec. streets	NO_2 diff(%)$_{s,m}$
CELES	75.87	0.398	4	10.30
BONAP	267.96	1.500	3	2.81
SOULT	177.51	0.498	5	10.03
ELYS	391.07	0.308	8	11.22
OPERA	315.12	0.681	5	7.68
HAUS	315.03	0.860	7	7.95
BP_EST	362.28	0.125	3	-0.46
BASCH	382.74	0.463	6	4.38

SinG and MUNICH background concentrations, higher are the differences between SinG and MUNICH street concentrations respectively.

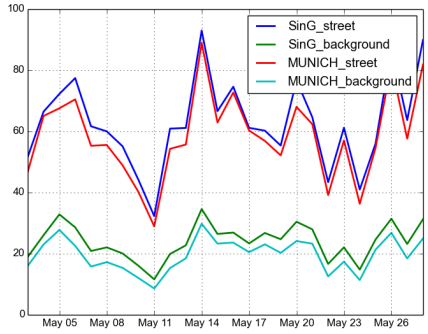

Figure 15. NO_2 ~~daily~~ daily-average concentrations [μg.m^{-3}] in the street and in the background at CELES traffic station.

However, as indicated in Table 7, the magnitude of the differences between SinG and MUNICH depends very much on the street: the lowest differences between SinG and MUNICH NO_2 concentrations are simulated at the stations BONAP and BP_EST, with differences below 3%, while the highest differences are simulated at the stations CELES, SOULT and ELYS, with differences around 10%.

To understand why the ~~dynamic~~ two-way coupling between the background and the streets differs depending on stations, the differences between SinG and MUNICH are analysed in terms of the ~~daily weighted~~ daily-weighted mass fluxes that influence the street concentrations. As detailed in section 2.2, the street concentrations are influenced by the vertical mass flux from/to background concentrations (Q_{vert}), but also the emission mass flux (Q_{emis}) and the mass fluxes from the street lateral

boundaries (Q_{inflow}, $Q_{outflow}$). ~~Daily weighted~~ Daily-weighted mass fluxes (qf_i) are calculated according to:

$$q_{f_i} = \frac{Q_i}{\sum Q_i}; \text{ with } \sum Q_i = Q_{inflow} + Q_{emis} + Q_{outflow} + Q_{vert} \quad (18)$$

with

$$\sum Q_i = Q_{inflow} + Q_{emis} + Q_{outflow} + Q_{vert} \quad (19)$$

Figure 16 shows the ~~daily~~ daily-weighted mass fluxes influencing the street concentrations at BONAP, CELES and BP_EST. At BONAP, advection (inlet and outlet fluxes in Figure 16) dominates over vertical transfer, probably because the value of α_r is high, indicating that the street is narrow. At BP_EST, Figure 16 indicates that vertical transfer is the dominant process. This dominance of vertical transfer is because the street is large and the value of α_r is low. Note that BP_EST station also presents a high emission flux, common data to both models SinG and MUNICH. Also, both BP_EST and BONAP present a low number of connected streets, which may indicate an inferior vertical mass flux intersections compared to other traffic stations. At CELES, where the value of α_r is intermediate, the inlet, outlet and vertical fluxes have the same order of magnitude, and the differences between MUNICH and SinG are larger than at BONAP and BP_EST stations.

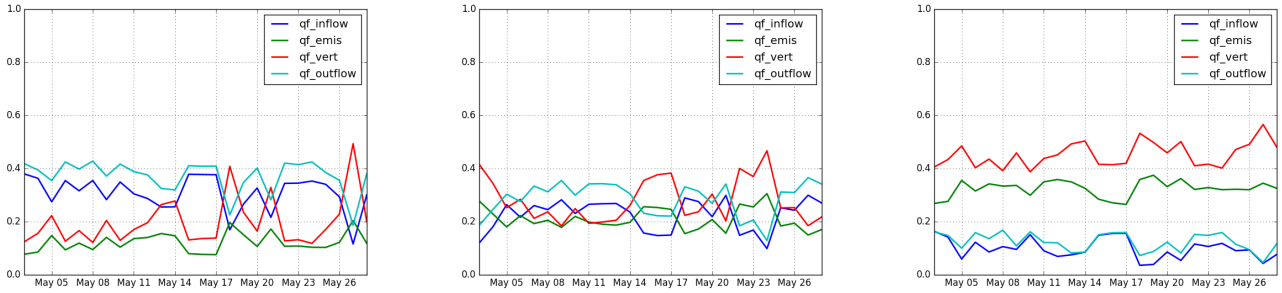

Figure 16. ~~Daily weighted~~ Daily-weighted mass fluxes of NO_2 at BONAP (left panel), CELES (middle panel) and BP_EST (right panel) traffic stations.

NO concentrations are less sensitive to the ~~dynamic~~ two-way coupling between local and regional scales than NO_2 concentrations, and the average concentrations simulated with SinG and MUNICH are very similar at all stations (as indicated in ~~Annexe~~Annex A2). This is explained by three reasons: (i) NO background concentrations are very low compared to NO concentrations in streets; (ii) NO has a short lifetime, as it quickly reacts to form NO_2; and (iii) NO concentrations in streets are mainly determined by direct emissions, which are the same in MUNICH and SinG simulations. Figure 17 shows the daily-weighted mass fluxes influencing the street concentrations at BONAP, CELES and BP_EST. At all three stations, the emission mass flux clearly dominates over the inlet/outlet and vertical mass fluxes, confirming the strong and local influence of NO emissions on NO concentrations.

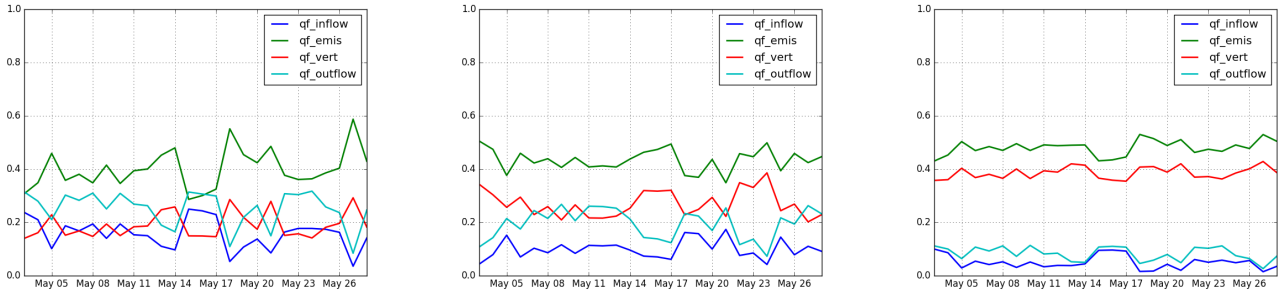

Figure 17. ~~Daily weighted~~ Daily-weighted mass flux of NO at BONAP (left panel), CELES (middle panel) and BP_EST (right panel) traffic stations.

To summarize, for NO concentrations, the two-way dynamic coupling between the regional and local scales tends not to be important. However, for NO_2 concentrations, it seems to be more important at stations with low to intermediate values of α_r, where the inlet, outlet and vertical fluxes have the same order of magnitude. In opposition, the ~~dynamic~~ two-way coupling seems to be less important at stations with low or high values of α_r, where either the vertical flux or the inlet/oulet fluxe dominates the other.

To better quantify the importance of the ~~dynamic~~ two-way coupling on the street concencentrations, the concentrations simulated with SinG and MUNICH in each street are compared over the whole Paris city street network. The relative differences between concentrations simulated with the two models are computed in each street. The average over all streets of these relative differences, as well as the minimum and maximum values are estimated and discussed below.

NO, NO_2 and NO_x average concentrations simulated with SinG, as well as the mean relative differences between SinG and MUNICH are represented in ~~Annexe~~Annex B, in Figure B1. As it was observed at traffic stations, the average NO_2 concentrations are larger with SinG than MUNICH for most streets in the network, with an average relative difference over all streets of about 7.5%. Although this relative difference is low, the maximum and the minimum differences are high and reach 63% and -28% respectively. The average NO concentrations is slightly lower with SinG than MUNICH, the average relative difference over all streets is low and about -0.85%. As for NO_2, for NO concentrations, there is a large variation between the maximum and minimum differences (58% and -35% respectively). Particularly, NO concentrations simulated with SinG are generally lower than those simulated with MUNICH in the center of the street network. However, in other places, such as the ring road, NO concentrations simulated with SinG are about 5% higher than those simulated with MUNICH. Similarly to NO_2, NO_x concentrations also presented low average differences between SinG and MUNICH, about 5% in the whole street-network, but with high maximum and minimun values (60% and -27% respectively). As discussed at the beginning of this section, relative differences between NO_2, NO and NO_x concentrations simulated with SinG and MUNICH are strongly correlated to the emissions in the street and to the street aspect ratio α_r. Therefore, large differences between SinG and MUNICH are observed in streets with high traffic emissions and intermediate to low values of α_r, such as in the ring road,

where the vertical mass transfer between streets and the background is important. The differences are less pronounced for NO concentrations, because of the short lifetime of NO.

As the majority of parisian streets presents an intermediate value of the street aspect ratio α_r, to better understand the influence of the street aspect ratio on the dynamic coupling, the variations of the relative differences between NO_2 and NO concentrations simulated with SinG and MUNICH with the street aspect ratio α_r are studied. For the different ranges of α_r encountered in the street network, and for different ranges of relative differences, Figure 18 represents the percentage of streets involved in the network. Thus, in the figure, the sum of each column is 100%. In accordance with Figure 14, NO_2 average concentrations are in general higher using SinG than using MUNICH. The relative difference is mostly between 2% and 30% for streets with α_r smaller than 1.8, and between 2% and 10% for streets with α_r larger than 1.8. The higher the value of α_r is, the lower is the variability of relative differences. However, even for α_r larger than 1.8, relative differences between 10% and 20% are relatively frequent (between 16% and 20% of the streets), indicating the influence of other factors than the street aspect ratios.

For NO, the average concentrations simulated with SinG are in general smaller than those simulated with MUNICH, mostly between 0% and -10%. As for NO_2, the variability of relative differences is higher for low to intermediate values of α_r.

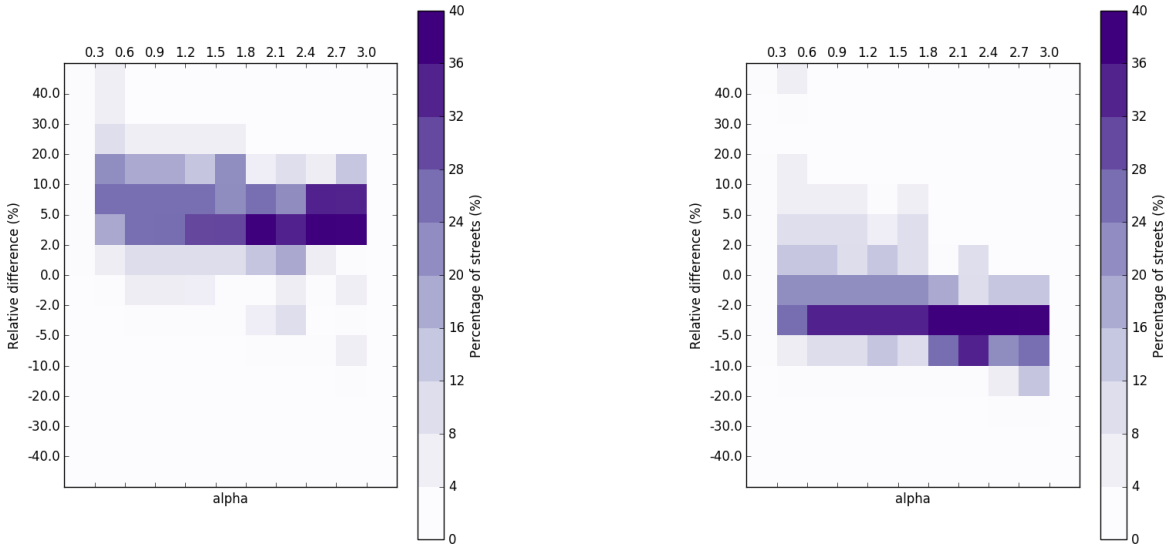

Figure 18. Percentage of streets (purple color) present in each α_r interval according to α_r values and the NO_2 (left panel) and NO (right panel) relative differences between pollutant concentrations calculated by SinG and MUNICH.

6.2 Regional scale

Figure B2 represents the spatial distribution of average background NO_2 and NO_x concentrations simulated with SinG, and the relative differences to those simulated with Polair3D. As indicated in section 5.2, background concentrations at the regional scale are influenced by the ~~dynamic~~ two-way coupling with the local scale. NO_2 concentration differences between SinG and Polair3D are in average 11%, with a maximum value equals to 34%. For NO_x concentrations, the relative differences are of the same order of magnitude than for NO_2, with an average and a maximum value equal to 15% and 42% respectively. NO concentrations are not shown in Figure B2, because they are very low at the regional scale.

For both NO_2 and NO_x, the most important differences between Polair3D and SinG background concentrations are observed at the ring road and in the north-west of Paris city. Similarly to the local scale, relative differences of concentrations simulated with SinG and MUNICH are higher in regions with high traffic emissions and where streets present an intermediate value of α_r, such as ELYS (see Figure 6). Note that, as mentioned in section 2.3, SinG output concentrations at the regional scale are an average of background and street concentrations in each grid cell. This justifies the higher differences between coupled and non-coupled simulations at the regional scale than at the local scale.

7 Conclusions

In this study, a Street-in-Grid (SinG) multi-scale simulation is performed over Paris city, with a two-way dynamic coupling between the local (street) and regional (background) scales. For Paris, 3819 streets are considered and different databases are used to determine the width and height of each street. A stationary approach may be used to compute pollutant concentrations in the streets, by performing a mass balance between emission, deposition and vertical and horizontal mass transfer. Although this approach is reasonable to estimate NO_x concentrations or the concentration of inert pollutants, it is not appropriate to compute the concentrations of reactive pollutants such as NO_2 or NO. A non-stationary dynamic approach ~~coupling finely chemistry and~~ was implemented, by solving with a second order numerical scheme the transport of pollutants ~~was implemented and~~ and chemistry. This approach proved to be numerically stable~~. It leads to~~, with a good agreement between observed and simulated concentrations of NO_2 and NO_x ~~concentrations that compare well to observations, both at the~~ at both regional and local scales.

In the streets, NO_x and NO_2 concentrations simulated by SinG compare well to measurements performed at traffic stations. For NO_2 concentrations, the statistical indicators obtained with SinG and the street model (MUNICH) respect the most strict performance criteria (Hanna and Chang, 2012) at traffic stations. However, NO concentrations are strongly underestimated at traffic stations located in streets that converge in big squares. This underestimation is probably due to the short life time of NO, for which the assumption of uniform concentrations in wide streets and big squares may not be ~~verified~~appropriate. At the regional scale, SinG performs also well ~~for~~ in simulating NO_x and NO_2 concentrations, and the most strict critera are respected at background stations.

The influence of the two-way dynamic coupling between the regional and local scales is assessed by comparing the concentrations simulated with SinG to those simulated with MUNICH. NO_x and NO_2 concentrations simulated with SinG and MUNICH are strongly correlated to traffic emissions, and the highest concentrations are observed in the ring road around Paris

city ("boulevard périphérique"), where emissions are the highest. Similarly, at both the local and regional scales, the influence of the dynamic coupling is larger in areas where traffic emissions are high. NO_2 concentrations simulated with SinG are in general larger than those simulated with MUNICH, especially in high emission areas, because the background concentrations in SinG are influenced by the high NO_x concentrations of the street network. The influence of the ~~dynamic~~ two-way coupling depends not only on the emission ~~strenght~~strength, but also on the aspect ratio (height over width) of the street. Although, on average over the streets of Paris, the influence of the ~~dynamic~~ two-way coupling on NO_2 concentrations in the street is only 7.5%, it can reach values as high as 63%. The influence of the ~~dynamic~~ two-way coupling on background regional NO_2 concentrations can be large as well: 11% on average over Paris with a maximum relative difference of 34%.

~~Further work will include the development of a new version of SinG to estimate particle-phase concentrations , taking into account the formation of secondary aerosols~~Because NO background concentrations are very low, and because of its short lifetime, NO concentrations are less sensitive to two-way dynamic coupling than NO_2.

Appendix A: Statistical parameters

A1 Definitions

- FB: Fractional bias
  $FB = 2\left(\frac{\overline{o}-\overline{c}}{\overline{o}+\overline{c}}\right)$
- MG: Geometric mean bias
  $MG = exp(\overline{ln(o)} - \overline{ln(c)})$
- NMSE: Normalized mean square error
  $NMSE = \frac{\overline{(o-c)^2}}{\overline{oc}}$
- VG: Geometric variance
  $VG = exp[\overline{(ln(o) - ln(c))^2}]$
- NAD: Normalised absolute difference
  $NAD = \frac{\overline{|c-o|}}{(\overline{c}+\overline{o})}$
- FAC2: Fraction of data that satisfy
  $0.5 \leq \frac{c}{o} \leq 2.0$
- ~~Correlation~~$cor = \frac{\overline{(o-\overline{o})(c-\overline{c})}}{\sigma_c \sigma_o}$

Where o and c represent the observed and simulated concentrations respectively.

A2 Statistical parameters at all traffic stations

		NO2								NO								NO_x							
		o	s	FB	MG	NMSE	VG	FAC2	NAD	o	s	FB	MG	NMSE	VG	FAC2	NAD	o	s	FB	MG	NMSE	VG	FAC2	NAD
	Polair3D	55.8	19.5	-0.96	0.36	1.41	3.02	0.04	0.48	49.6	3.0	-1.77	0.06	18.97	1590.06	0.00	0.88	131.5	24.1	-1.38	0.19	4.50	15.44	0.04	0.69
CELES	MUNICH	55.8	59.3	0.06	1.10	0.06	1.10	0.96	0.10	49.6	52.0	0.05	1.18	0.19	1.35	0.80	0.18	131.5	139.0	0.05	1.14	0.12	1.20	0.96	0.14
	SinG	55.8	64.0	0.13	1.19	0.08	1.13	0.96	0.12	49.6	51.6	0.04	1.17	0.21	1.37	0.80	0.19	131.5	143.1	0.08	1.18	0.13	1.23	0.88	0.15
	Polair3D	46.2	21.0	-0.75	0.45	0.72	1.98	0.20	0.37	43.7	3.4	-1.71	0.07	11.76	818.11	0.00	0.85	113.1	26.2	-1.24	0.23	2.71	9.41	0.00	0.62
BONAP	MUNICH	46.2	53.6	0.15	1.15	0.07	1.07	1.00	0.11	43.7	25.9	-0.51	0.58	0.37	1.47	0.68	0.25	113.1	93.4	-0.19	0.81	0.09	1.10	1.00	0.12
	SinG	46.2	54.3	0.16	1.17	0.07	1.07	1.00	0.11	43.7	25.0	-0.54	0.56	0.41	1.52	0.68	0.27	113.1	92.7	-0.20	0.81	0.09	1.10	1.00	0.12
	Polair3D	40.4	20.7	-0.64	0.51	0.55	1.63	0.48	0.32	19.6	3.3	-1.41	0.19	5.52	18.29	0.00	0.70	70.3	25.8	-0.92	0.38	1.33	2.72	0.12	0.46
SOULT	MUNICH	40.4	42.8	0.06	1.05	0.07	1.07	1.00	0.10	19.6	20.5	0.04	1.13	0.18	1.19	0.92	0.17	70.3	74.3	0.05	1.08	0.09	1.09	1.00	0.12
	SinG	40.4	46.1	0.13	1.14	0.08	1.08	1.00	0.11	19.6	20.1	0.02	1.12	0.16	1.17	0.92	0.16	70.3	77.0	0.09	1.12	0.08	1.09	1.00	0.12
	Polair3D	51.0	23.3	-0.74	0.45	0.74	2.02	0.32	0.37	38.4	4.1	-1.61	0.11	9.01	156.53	0.00	0.80	109.8	29.6	-1.15	0.27	2.31	6.27	0.12	0.57
ELYS	MUNICH	51.0	45.5	-0.11	0.89	0.07	1.08	1.00	0.12	38.4	19.4	-0.66	0.53	0.76	1.80	0.56	0.35	109.8	75.2	-0.37	0.70	0.26	1.27	0.84	0.22
	SinG	51.0	49.8	-0.02	0.97	0.05	1.05	1.00	0.09	38.4	18.5	-0.70	0.51	0.83	1.86	0.40	0.36	109.8	78.1	-0.33	0.73	0.22	1.27	0.84	0.20
	Polair3D	74.3	23.6	-1.03	0.31	1.55	4.00	0.00	0.51	81.1	4.1	-1.80	0.05	19.20	7472.94	0.00	0.90	198.5	30.0	-1.47	0.15	5.11	38.59	0.00	0.73
OPERA	MUNICH	74.3	56.7	-0.26	0.75	0.11	1.13	1.00	0.14	81.1	29.5	-0.93	0.36	1.27	3.04	0.16	0.46	198.5	102.1	-0.64	0.51	0.54	1.67	0.48	0.32
	SinG	74.3	60.3	-0.20	0.80	0.08	1.09	1.00	0.12	81.1	27.7	-0.98	0.34	1.43	3.41	0.08	0.49	198.5	102.8	-0.63	0.51	0.52	1.64	0.52	0.31
	Polair3D	56.1	23.3	-0.82	0.42	0.98	2.25	0.28	0.41	37.2	4.0	-1.60	0.12	10.00	109.89	0.00	0.80	112.8	29.5	-1.16	0.27	2.67	6.08	0.08	0.58
HAUS	MUNICH	56.1	51.8	-0.08	0.94	0.10	1.07	1.00	0.12	37.2	21.2	-0.54	0.64	0.81	1.62	0.68	0.31	112.8	84.4	-0.28	0.78	0.29	1.22	0.88	0.20
	SinG	56.1	55.5	-0.01	1.00	0.09	1.07	1.00	0.11	37.2	19.8	-0.60	0.60	0.92	1.71	0.60	0.33	112.8	86.0	-0.27	0.80	0.28	1.21	0.88	0.20
	Polair3D	70.7	24.2	-0.97	0.37	1.79	3.40	0.32	0.49	88.6	4.5	-1.80	0.06	26.11	2997.77	0.00	0.90	206.3	31.2	-1.47	0.18	6.89	29.36	0.12	0.73
BP_EST	MUNICH	70.7	81.7	0.14	1.26	0.20	1.38	0.80	0.18	88.6	84.5	-0.04	1.27	0.43	2.29	0.64	0.26	206.3	211.4	0.02	1.24	0.31	1.77	0.64	0.22
	SinG	70.7	80.3	0.12	1.24	0.20	1.38	0.80	0.18	88.6	81.5	-0.08	1.22	0.45	2.27	0.56	0.27	206.3	205.2	-0.005	1.21	0.32	1.76	0.64	0.23
	Polair3D	78.4	20.0	-1.18	0.25	2.37	7.42	0.00	0.59	98.1	3.1	-1.86	0.03	30.1	115444.50	0.00	0.93	228.9	25.0	-1.60	0.11	7.82	157.58	0.00	0.80
BASCH	MUNICH	78.4	50.0	-0.44	0.63	0.28	1.33	0.80	0.22	98.1	26.8	-1.14	0.27	2.16	5.79	0.00	0.57	228.9	91.1	-0.86	0.39	1.04	2.55	0.20	0.43
	SinG	78.4	51.5	-0.41	0.65	0.25	1.30	0.80	0.20	98.1	25.7	-1.16	0.26	2.32	6.39	0.00	0.58	228.9	90.9	-0.86	0.39	1.04	2.55	0.16	0.43

Appendix B: Concentration maps - local and regional scales

B1 Local scale

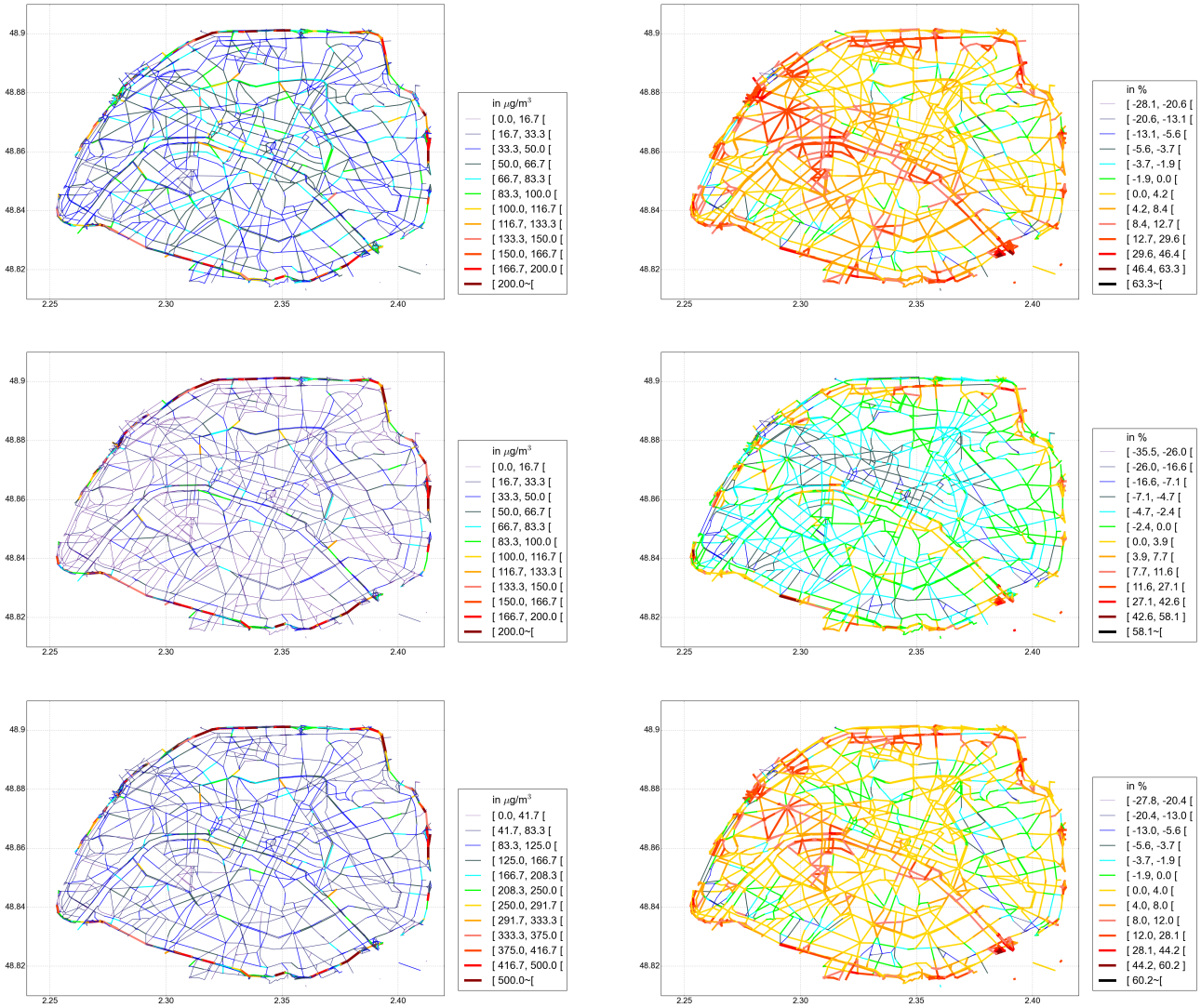

Figure B1. NO_2 (top panels), NO (middle panels) and NO_x (bottom panels) concentrations simulated over Paris with SinG (left panels) and relative differences between SinG and MUNICH (right panels).

B2 Regional scale

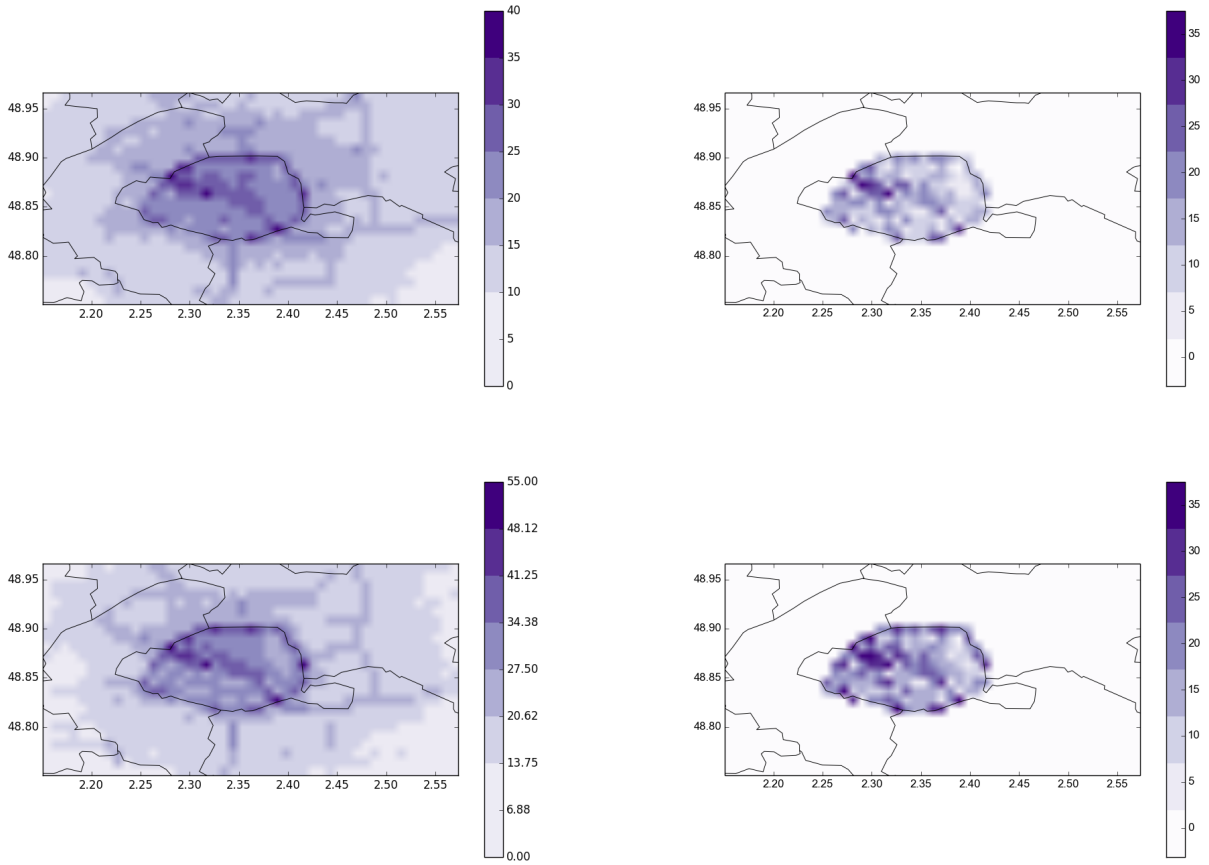

Figure B2. NO_2 (top panels) and NO_x (bottom panels) concentrations simulated over Paris with SinG (left panels) and relative differences between SinG and Polair3D, in % (right panels).

Acknowledgements. This study was partially funded by the Departement of green spaces and environment of Paris City. The authors also thank Aiparif and the ANSES (french agency for food safety, environment and labor) working group on ambiant particulate matter for the trafic emission informations. Dr Yelva Roustan, Fabrice Dugay and Olivier Sanchez are gratefully acknowledged for discussions.

References

Abdallah, C., Afif, C., El Masri, N., Öztürk, F., Keleş, M., and Sartelet, K.: A first annual assessment of air quality modeling over Lebanon using WRF/Polyphemus, Atmos. Pol. Res., 9, 643–654, 2018.

Ascher, U. and Petzold, L.: Computer Methods for Ordinary Differential Equations and Differential-Algebraic Equations, ISBN 978-0-89871-412-8., Philadelphia: Society for Industrial and Applied Mathematics, 1998.

Benson, P. E.: Caline4 - A dispersion model for predictiong air pollutant concentrations near roadways, Tech. rep., 1984.

Berkowicz, R.: OSPM - A parameterised street pollution model, Environ. Monit. Assess., 65, 323–331, 2000.

Berkowicz, R., Hertel, O., Larsen, S. E., Sørensen, N. N., and Nielsen, M.: Modelling traffic pollution in streets, 1997.

Bieser, J., Aulinger, A., Matthias, V., Quante, M., and van Der Gon, H. D.: Vertical emission profiles for Europe based on plume rise calculations, Environ. Pollut., 159, 2935–2946, 2011.

Boutahar, J., Lacour, S., Mallet, V., Quélo, D., Roustan, Y., and Sportisse, B.: Development and validation of a fully modular platform for numerical modelling of air pollution: POLAIR, Int. J. Environ. Pollut., 22, 17–28, 2004.

Brandt, J., Christensen, J., Frohn, L., and Berkowicz, R.: Operational air pollution forecasts from regional scale to urban street scale. Part 1: System description, Phys. Chem. Earth, 26, 781–786, 2001a.

Brandt, J., Christensen, J., Frohn, L., and Berkowicz, R.: Operational air pollution forecasts from regional scale to urban street scale. Part 2: performance evaluation, Phys. Chem. Earth, 26, 825–830, 2001b.

Brandt, J., Christensen, J. H., Frohn, L. M., Palmgren, F., Berkowicz, R., and Zlatev, Z.: Operational air pollution forecasts from European to local scale, Atmos. Environ., 35, S91–S98, 2001c.

Briant, R. and Seigneur, C.: Multi-scale modeling of roadway air quality impacts: Development and evaluation of a Plume-in-Grid model, Atmos. Environ., 68, 162–173, 2013.

Brønnum-Hansen, H., Bender, A. M., Andersen, Z. J., Sørensen, J., Bønløkke, J. H., Boshuizen, H., Becker, T., Diderichsen, F., and Loft, S.: Assessment of impact of traffic-related air pollution on morbidity and mortality in Copenhagen municipality and the health gain of reduced exposure, Environ. Int., 121, 973–980, 2018.

Byun, D. and Ching, J.: Science algorithms of the EPA models-3 community multiscale air quality model (CMAQ) modeling system, Washington, DC: US Env. Protec. Agency, 1999.

Cariolle, D., Caro, D., Paoli, R., Hauglustaine, D., Cuénot, B., Cozic, A., and Paugam, R.: Parameterization of plume chemistry into large-scale atmospheric models: Application to aircraft NOx emissions, J. Geophys. Res.-Atmos., 114, 2009.

Chen, Z., Cui, L., Cui, X., Li, X., Yu, K., Yue, K., Dai, Z., Zhou, J., Jia, G., and Zhang, J.: The association between high ambient air pollution exposure and respiratory health of young children: A cross sectional study in Jinan, China, Sci. Total Environ., 656, 740–749, 2019.

Chin, M., Ginoux, P., Kinne, S., Torres, O., Holben, B. N., Duncan, B. N., Martin, R. V., Logan, J. A., Higurashi, A., and Nakajima, T.: Tropospheric aerosol optical thickness from the GOCART model and comparisons with satellite and Sun photometer measurements, J. Atmos. Sci., 59, 461–483, 2002.

Couvidat, F., Kim, Y., Sartelet, K., Seigneur, C., Marchand, N., and Sciare, J.: Modeling secondary organic aerosol in an urban area: application to Paris, France, Atmos. Chem. Phys., 13, 983–996, 2013.

De Marco, A., Proietti, C., Anav, A., Ciancarella, L., D'Elia, I., Fares, S., Fornasier, M. F., Fusaro, L., Gualtieri, M., Manes, F., et al.: Impacts of air pollution on human and ecosystem health, and implications for the national emission ceilings directive: Insights from Italy, Environ. Int., 125, 320–333, 2019.

Eerens, H., Sliggers, C., and Van den Hout, K.: The CAR model: The dutch method to determine city street air quality, Atmos. Environ., 27, 389–399, 1993.

Emmons, L. K., Walters, S., Hess, P. G., Lamarque, J.-F., Pfister, G. G., Fillmore, D., Granier, C., Guenther, A., Kinnison, D., Laepple, T., et al.: Description and evaluation of the Model for Ozone and Related chemical Tracers, version 4 (MOZART-4), Geosci. Model Dev., 2010.

Freitas, S. R., Longo, K. M., Chatfield, R., Latham, D., Silva Dias, M., Andreae, M., Prins, E., Santos, J., Gielow, R., and Carvalho Jr, J.: Including the sub-grid scale plume rise of vegetation fires in low resolution atmospheric transport models, Atmos. Chem. Phys., 7, 3385–3398, 2007.

Hanna, S. and Chang, J.: Acceptance criteria for urban dispersion model evaluation, Meteorol. Atmos. Phys., 116, 133–146, 2012.

Herring, S. and Huq, P.: A review of methodology for evaluating the performance of atmospheric transport and dispersion models and suggested protocol for providing more informative results, Fluids, 3, 20, 2018.

Hood, C., MacKenzie, I., Stocker, J., Johnson, K., Carruthers, D., Vieno, M., and Doherty, R.: Air quality simulations for London using a coupled regional-to-local modelling system, Atmos. Chem. Phys., 18, 11 221–11 245, 2018.

Hotchkiss, R. and Harlow, F.: Air pollution transport in street canyons. Report by Los Alamos scientific laboratory for US Environmental Protection Agency, Tech. rep., EPA-R4-73-029, NTIS PB-233 252, 1973.

Jensen, S. S., Ketzel, M., Becker, T., Christensen, J., Brandt, J., Plejdrup, M., Winther, M., Nielsen, O.-K., Hertel, O., and Ellermann, T.: High resolution multi-scale air quality modelling for all streets in Denmark, Transp. Res. Part D, 52, 322–339, 2017.

Johnson, W., Ludwig, F., Dabberdt, W., and Allen, R.: An urban diffusion simulation model for carbon monoxide, J. Air Pollut. Control Assoc., 23, 490–498, 1973.

Karamchandani, P., Seigneur, C., Vijayaraghavan, K., and Wu, S.-Y.: Development and application of a state-of-the-science plume-in-grid model, J. Geophys. Res.-Atmos., 107, ACH–12, 2002.

Karamchandani, P., Vijayaraghavan, K., Chen, S.-Y., Seigneur, C., and Edgerton, E. S.: Plume-in-grid modeling for particulate matter, Atmos. Environ., 40, 7280–7297, 2006.

Karamchandani, P., Vijayaraghavan, K., and Yarwood, G.: Sub-grid scale plume modeling, Atmosphere, 2, 389–406, 2011.

Katoto, P. D., Byamungu, L., Brand, A. S., Mokaya, J., Strijdom, H., Goswami, N., De Boever, P., Nawrot, T. S., and Nemery, B.: Ambient air pollution and health in Sub-Saharan Africa: Current evidence, perspectives and a call to action., Environ. Res., 2019.

Kim, Y., Seigneur, C., and Duclaux, O.: Development of a plume-in-grid model for industrial point and volume sources: application to power plant and refinery sources in the Paris region, Geosci. Model Dev., 7, 569–585, 2014.

Kim, Y., Sartelet, K., Raut, J.-C., and Chazette, P.: Influence of an urban canopy model and PBL schemes on vertical mixing for air quality modeling over Greater Paris, Atmos. Environ., 107, 289–306, 2015.

Kim, Y., Wu, Y., Seigneur, C., and Roustan, Y.: Multi-scale modeling of urban air pollution: development and application of a Street-in-Grid model (v1. 0) by coupling MUNICH (v1. 0) and Polair3D (v1. 8.1), Geosci. Model Dev., 11, 611, 2018.

Korsakissok, I., Mallet, V., and Quélo, D.: Modeling of dispersion and scavenging in the Polyphemus platform. Applications to passive tracers, Rapport technique, 2006.

Landsberg, H. E.: The urban climate, vol. 28, Academic press, 1981.

Lee, S., Yoo, H., and Nam, M.: Impact of the clean air act on air pollution and infant health: Evidence from South Korea, Econom. Lett., 168, 98–101, 2018.

Mallet, V., Quélo, D., Sportisse, B., Ahmed de Biasi, M., Debry, E., Korsakissok, I., Wu, L., Roustan, Y., Sartelet, K., Tombette, M., et al.: The air quality modeling system Polyphemus, Atmos. Chem. Phys., 7, 5479–5487, 2007.

McHugh, C., Carruthers, D., and Edmunds, H.: ADMS–Urban: An air quality management system for traffic, domestic and industrial pollution, Int. J. Environ. Pollut., 8, 666–674, 1997.

Mensink, C., De Ridder, K., Lewyckyj, N., Delobbe, L., Janssen, L., and Van Haver, P.: Computational aspects of air quality modelling in urban regions using an optimal resolution approach (AURORA), in: International Conference on Large-Scale Scientific Computing, pp. 299–308, Springer, 2001.

Menut, L., Bessagnet, B., Khvorostyanov, D., Beekmann, M., Blond, N., Colette, A., Coll, I., Curci, G., Foret, G., Hodzic, A., et al.: CHIMERE 2013: A model for regional atmospheric composition modelling, Geosci. Model Dev., 6, 981–1028, 2014.

Morris, R. E., Yarwood, G., Emery, C. A., and Wilson, G. M.: Recent advances in photochemical air quality modeling using the CAMx Model: Current update and ozone modeling of point source impacts, in: Air and Waste Management Association Meeting, Paper, vol. 43180, 2002a.

Morris, R. E., Yarwood, G., and Wagner, A.: Recent advances in CAMx air quality modelling, in: Air pollution modelling and simulation, pp. 79–88, Springer, 2002b.

Pourchet, A., Mallet, V., Quélo, D., and Sportisse, B.: Some numerical issues in Chemistry-Transport Models - a comprehensive study with the Polyphemus/Polair3D platform, Rapport technique, 26, 2005.

Rissman, J., Arunachalam, S., Woody, M., West, J. J., BenDor, T., and Binkowski, F. S.: A plume-in-grid approach to characterize air quality impacts of aircraft emissions at the Hartsfield–Jackson Atlanta international airport, Atmos. Chem. Phys., 13, 9285–9302, 2013.

Rosenbrock, H.: Some general implicit processes for the numerical solution of differential equations, The Computer Journal, 5, 329–330, 1963.

Royer, P., Chazette, P., Sartelet, K., Zhang, Q., Beekmann, M., and Raut, J.-C.: Comparison of lidar-derived PM10 with regional modeling and ground-based observations in the frame of MEGAPOLI experiment, Atmos. Chem. Phys., 11, 10 705–10 726, https://doi.org/10.5194/acp-11-10705-2011, 2011.

Sandu, A., Verwer, J., Blom, J., Spee, E., Carmichael, G., and Potra, F.: Benchmarking stiff ode solvers for atmospheric chemistry problems II: Rosenbrock solvers, Atmos. Environ., 31, 3459–3472, 1997.

Sartelet, K., Hayami, H., Albriet, B., and Sportisse, B.: Development and preliminary validation of a modal aerosol model for tropospheric chemistry: MAM, Aerosol Sci. Technol., 40, 118–127, 2006.

Sartelet, K., Debry, E., Fahey, K., Roustan, Y., Tombette, M., and Sportisse, B.: Simulation of aerosols and gas-phase species over Europe with the POLYPHEMUS system: Part I—Model-to-data comparison for 2001, Atmos. Environ., 41, 6116–6131, 2007.

Sartelet, K., Zhu, S., Moukhtar, S., André, M., André, J., Gros, V., Favez, O., Brasseur, A., and Redaelli, M.: Emission of intermediate, semi and low volatile organic compounds from traffic and their impact on secondary organic aerosol concentrations over Greater Paris, Atmos. Environ., 180, 126–137, 2018.

Sartelet, K. N., Couvidat, F., Seigneur, C., and Roustan, Y.: Impact of biogenic emissions on air quality over Europe and North America, Atmos. Environ., 53, 131–141, 2012.

Seigneur, C., Tesche, T., Roth, P. M., and Liu, M.-K.: On the treatment of point source emissions in urban air quality modeling, Atmos. Environ., 17, 1655–1676, 1983.

Sharma, N., Gulia, S., Dhyani, R., and Singh, A.: Performance evaluation of CALINE 4 dispersion model for an urban highway corridor in Delhi, J. Sci. Ind. Res., 72, 521–530, 2013.

Skamarock, W. C., Klemp, J. B., Dudhia, J., Gill, D. O., Barker, D. M., Duda, M. G., Huang, X.-Y., Wang, W., and Powers, J. G.: A description of the advanced research WRF version 3, NCAR Technical Note, NCAR: Boulder, CO, USA, 2008.

Soulhac, L., Perkins, R. J., and Salizzoni, P.: Flow in a street canyon for any external wind direction, Bound.-Lay. Meteorol., 126, 365–388, 2008.

Soulhac, L., Garbero, V., Salizzoni, P., Mejean, P., and Perkins, R.: Flow and dispersion in street intersections, Atmos. Environ., 43, 2981–2996, 2009.

Soulhac, L., Salizzoni, P., Cierco, F.-X., and Perkins, R.: The model SIRANE for atmospheric urban pollutant dispersion: Part I, presentation of the model, Atmos. Environ., 45, 7339–7395, 2011.

Soulhac, L., Salizzoni, P., Mejean, P., Didier, D., and Rios, I.: The model SIRANE for atmospheric urban pollutant dispersion: Part II, validation of the model on a real case study, Atmos. Environ., 49, 320–337, 2012.

Soulhac, L., Lamaison, G., Cierco, F.-X., Salem, N. B., Salizzoni, P., Mejean, P., Armand, P., and Patryl, L.: SIRANERISK: Modelling dispersion of steady and unsteady pollutant releases in the urban canopy, Atmos. Environ., 140, 242–260, 2016.

Soulhac, L., Nguyen, C. V., Volta, P., and Salizzoni, P.: The model SIRANE for atmospheric urban pollutant dispersion: Part III, Validation against NO2 yearly concentration measurements in a large urban agglomeration, Atmos. Environ., 167, 377–388, 2017.

Sportisse, B. and Du Bois, L.: Numerical and theoretical investigation of a simplified model for the parameterization of below-cloud scavenging by falling raindrops, Atmos. Environ., 36, 5719–5727, 2002.

Stocker, J., Hood, C., Carruthers, D., and McHugh, C.: ADMS–Urban: Developments in modelling dispersion from the city scale to the local scale, Int. J. Environ. Pollut., 50, 308–316, 2012.

Vieno, M., Dore, A. J., Wind, P., Di Marco, C., Nemitz, E., Phillips, G., Tarrasón, L., and Sutton, M. A.: Application of the EMEP unified model to the UK with a horizontal resolution of 5× 5 km 2, in: Atmospheric Ammonia, pp. 367–372, Springer, 2009.

Vijayaraghavan, K., Karamchandani, P., and Seigneur, C.: Plume-in-grid modeling of summer air pollution in Central California, Atmos. Environ., 40, 5097–5109, 2006.

Vijayaraghavan, K., Karamchandani, P., Seigneur, C., Balmori, R., and Chen, S.-Y.: Plume-in-grid modeling of atmospheric mercury, J. Geophys. Res.-Atmos., 113, 2008.

Voss, D. A. and Khaliq, A.-Q. M.: Parallel Rosenbrock methods for chemical systems, Comput. Chem., 25, 101–107, 2001.

WHO: Air quality guidelines for particulate matter, ozone, nitrogen dioxide and sulfur dioxide: global update 2005. Summary of risk assessment, in: WHO Air quality guidelines, World Health Organization, 2006.

Yamartino, R. J. and Wiegand, G.: Development and evaluation of simple models for the flow, turbulence and pollutant concentration fields within an urban street canyon, Atmos. Environ., 20, 2137–2156, 1986.

Yarwood, G., Rao, S., Yocke, M., and Whitten, G.: Updates to the carbon bond chemical mechanism: CB05, Final report to the US EPA, RT-0400675, 8, 2005.

Zhang, L., Brook, J., and Vet, R.: A revised parameterization for gaseous dry deposition in air-quality models, Atmos. Chem. Phys., 3, 2067–2082, 2003.

Zhang, Y., Pan, Y., Wang, K., Fast, J. D., and Grell, G. A.: WRF/Chem-MADRID: Incorporation of an aerosol module into WRF/Chem and its initial application to the TexAQS2000 episode, J. Geophys. Res.-Atmos., 115, 2010.

Zhu, S., Sartelet, K., Zhang, Y., and Nenes, A.: Three-dimensional modeling of the mixing state of particles over Greater Paris, J. Geophys. Res.-Atmos., 121, 5930–5947, 2016a.

Zhu, S., Sartelet, K. N., Healy, R. M., and Wenger, J. C.: Simulation of particle diversity and mixing state over Greater Paris: a model–measurement inter-comparison, Faraday Discuss., 189, 547–566, 2016b.